DISCLAIMER

This report was prepared as an account of work sponsored by an agency of the United States Government. Neither the United States Government nor any agency thereof, nor any of their employees, makes any warranty, express or implied, or assumes any legal liability or responsibility for the accuracy, completeness, or usefulness of any information, apparatus, product, or process disclosed, or represents that its use would not infringe privately owned rights. Reference herein to any specific commercial product, process, or service by trade name, trademark, manufacturer, or otherwise does not necessarily constitute or imply its endorsement, recommendation, or favoring by the United States Government or any agency thereof. The views and opinions of authors expressed herein do not necessarily state or reflect those of the United States Government or any agency thereof. Reference herein to any social initiative (including but not limited to Diversity, Equity, and Inclusion (DEI); Community Benefits Plans (CBP); Justice 40; etc.) is made by the Author independent of any current requirement by the United States Government and does not constitute or imply endorsement, recommendation, or support by the United States Government or any agency thereof.

SANDIA REPORT
SAND2025-04942
Printed April 2025

Sandia National Laboratories

Hydrogen Plus Other Alternative Fuels Risk Assessment Models (HyRAM+) Version 6.0 Technical Reference Manual

Updated by: Brian D. Ehrhart, Ethan S. Hecht, and Michael C. Devin

Previous Contributors (alphabetical): Myra L. Blaylock, Erin E. Carrier, Brian D. Ehrhart, Katrina M. Groth, Ethan S. Hecht, John T. Reynolds, and Benjamin B. Schroeder

Prepared by
Sandia National Laboratories
Albuquerque, New Mexico 87185
Livermore, California 94550

Issued by Sandia National Laboratories, operated for the United States Department of Energy by National Technology & Engineering Solutions of Sandia, LLC.

Available to DOE and DOE contractors from

U.S. Department of Energy
Office of Scientific and Technical Information
P.O. Box 62
Oak Ridge, TN 37831

Telephone: (865) 576-8401
Facsimile: (865) 576-5728
E-Mail: reports@osti.gov
Online ordering: http://www.osti.gov/scitech

Available to the public from

U.S. Department of Commerce
National Technical Information Service
5301 Shawnee Road
Alexandria, VA 22312

Telephone: (800) 553-6847
Facsimile: (703) 605-6900
E-Mail: orders@ntis.gov
Online order: https://classic.ntis.gov/help/order-methods

ABSTRACT

The HyRAM+ software is an open-source toolkit that provides publicly available models and default input values to enable straightforward and consistent safety assessments for hydrogen and other alternative fuel systems, such as natural gas and propane. The HyRAM+ quantitative risk assessment calculation incorporates annual likelihood of leaks or failures for both compressed gaseous and liquefied flammable fuels, as well as probabilistic models for the effects of heat flux and overpressure. HyRAM+ contains experimentally validated models of various aspects of release behavior, including orifice flow, unignited dispersion, and flame behavior. This document provides a description of the methodology and models contained in HyRAM+ version 6.0. The most significant changes for HyRAM+ version 6.0 from HyRAM+ version 5.1 are the new graphical user interface which allows installation on macOS in addition to Windows, new default leak frequencies for filters, and the addition of uncertainty quantification to the back-end Python package.

This page intentionally left blank.

ACKNOWLEDGEMENTS

This report describes HyRAM+, a revised version of the HyRAM code, which itself was built upon the previous work of many others. The authors therefore wish to thank Katrina Groth, John Reynolds, Greg Walkup, Isaac Ekoto, Erin Carrier, Alice Muna, Chris LaFleur, and Myra Blaylock for their past contributions to HyRAM. The authors also wish to thank Ben Liu and Ben Schroeder of Sandia and Cianan Sims of Sims Industries for their contributions to the current HyRAM+ code.

This revision to HyRAM+ was supported by the U.S. Department of Energy (DOE) Office of Technology Transitions (OTT) Technology Commercialization Fund (TCF) Core Laboratory Infrastructure for Market Readiness (CLIMR) program, and the U.S. DOE Office of Energy Efficiency (EERE) Hydrogen and Fuel Cell Technologies Office (HFTO) Safety Codes and Standards sub-program. The Hydrogen Fuel Cell Partnership (H2FCP) and the Electric Power Research Institute (EPRI) provided in-kind reviews and feedback for the development of HyRAM+ v6.0. Past versions of HyRAM/HyRAM+ were supported by the U.S. DOE EERE HFTO, the U.S. DOE EERE Vehicle Technologies Office (VTO) and the U.S. Department of Transportation (DOT) Pipeline and Hazardous Materials Safety Administration (PHMSA).

The authors wish to thank Dusty Brooks, Melissa Louie, Kristin Hertz, and Chris LaFleur from Sandia National Laboratories for their review of this document.

Finally, the authors gratefully acknowledge the many productive discussions with users, other researchers, and the various stakeholders who have provided insight and feedback for this work.

This page intentionally left blank.

CONTENTS

LIST OF FIGURES

This page intentionally left blank.

LIST OF TABLES

This page intentionally left blank.

ACRONYMS AND TERMS

AIR average individual risk

BST Baker-Stehlow-Tang

FAR fatal accident rate

FTC failure to close

FTO failure to open

HSE U.K. Health and Safety Executive

HyRAM Hydrogen Risk Assessment Models

HyRAM+ Hydrogen Plus Other Alternative Fuels Risk Assessment Models

MW molecular weight

PLL potential loss of life

PRD pressure relief device

QRA quantitative risk assessment

SI International System of Units

TNO Netherlands Organisation for Applied Scientific Research

TNT trinitrotoluene

UQ uncertainty quantification

This page intentionally left blank.

1. INTRODUCTION

The Hydrogen Plus Other Alternative Fuels Risk Assessment Models (HyRAM+) software is a toolkit that provides publicly available models and default input values to enable straightforward and consistent safety assessments for hydrogen and other alternative fuel (i.e., natural gas and propane) systems. The HyRAM+ quantitative risk assessment (QRA) calculation incorporates annual frequencies and probabilities of leaks or failures for both compressed gaseous and liquefied fuels, as well as probabilistic models for the effects of heat flux and overpressure. HyRAM+ also contains experimentally validated models of various aspects of release behavior, including orifice flow, unignited dispersion, and flame behavior. Installation files, links to the source code, and documentation downloads are available at the HyRAM+ website: `https://hyram.sandia.gov`.

1.1. HyRAM+ Design Goals and Limitations

HyRAM+ was originally designed for the hydrogen safety, codes, and standards community to provide risk-informed insights for stakeholders by enabling risk and harm metric calculations for user-defined systems [1–4]. HyRAM+ contains default inputs and reduced-order models, which users may use as a basis for comparing different system designs. Default input values are able to be replaced with more specific information based on the user's needs. Reduced-order models use simplifying assumptions to approximate behavior much more quickly than more complex high-fidelity models. The physics models contained in HyRAM+ have been validated against available experimental data [5–8]. There are some phenomena for which experimental validation is not available. In these cases, HyRAM+ provides multiple different model options that can be used to compare the effects of alternative models.

1.2. About This Report

This report provides technical documentation of the equations, models, and default values implemented in HyRAM+ version 6.0. HyRAM+ version 6.0 is a revised version of the software, and this report has a lot of similar content due to similarities between the previous versions of this software, as well as several versions of the previously named Hydrogen Risk Assessment Models (HyRAM) software. This report and the HyRAM+ software build off the models and implementations from those earlier versions [3, 9–15]. The models and default values are included in this report to maintain a complete record of the state of the software for version 6.0, even if some of these models and values are unchanged from a previous version of the software.

1.3. Summary of Changes Made

HyRAM+ is an open source software, meaning that changes to the code can be observed directly[1]. However, a summary of major changes to the models is included here for ease of reference.

The most significant changes for HyRAM+ version 6.0 from HyRAM+ version 5.1 are the new graphical user interface which allows installation on macOS in addition to the previously supported Windows operating system, new default leak frequencies for filters (see Section 2.1.3), and the addition of uncertainty quantification to the back-end Python package (see Section 2.6).

Other changes include:

- Added unconfined overpressure tests to the validation test suite
- Sped up QRA analysis by skipping unneeded consequence calculations for zero-risk conditions
- Modified isentropic blowdown calculation to use interpolating functions, which improves calculation speed by limiting calls to CoolProp
- Removed facility length and width for QRA plots, which was previously unused in calculations
- Corrected the flammable mass calculation in the Jet class, which was previously being undercalculated by missing some flammable mass near the fuel-rich region
- Added additional help text and references to Technical Reference Manual sections in graphical user interface

[1] More detailed changes are given in the source code changelog: `https://github.com/sandialabs/hyram/blob/master/CHANGELOG.md`

2. QUANTITATIVE RISK ASSESSMENT

Risk can be described by a set of hazard exposure scenarios, the likelihood of occurrence of these scenarios, and the consequences associated with each scenario [16]. In HyRAM+, the number of fatalities is the life safety metric of interest in the QRA. The consequences and fatality risk of jet flames and overpressures are estimated for different release sizes, each of which can be predicted to occur with different frequencies [1–4, 17]. These risk calculations utilize some of the physics models in HyRAM+ to estimate the physical release behavior (see Section 3).

HyRAM+ calculates the risk for release (leak) sizes of 0.01%, 0.1%, 1%, 10%, or 100% of pipe flow area [1–4]. These release sizes are relative to the pipe flow area (A) as shown in Equation 1, where C_d is the discharge coefficient, and d is the inner diameter of the pipe. The leak sizes are all relative to the size of the interconnecting piping, so leaks from all components are assumed to be the same size.

$$A = \frac{\pi}{4} C_d d^2 \tag{1}$$

2.1. Frequency of a Release

HyRAM+ estimates the annual frequency of a release for release sizes of 0.01%, 0.1%, 1%, 10%, or 100% of pipe flow area [1–4]. The annual frequency of a release ($f_{\text{Release},s}$) for each of the four smallest release sizes (s = 0.01%, 0.1%, 1%, and 10%) is based on the annual frequency of random leaks ($f_{\text{Random Releases},s}$, see Section 2.1.1), as shown in Equation 2 [3, 17].

$$f_{\text{Release},s} = f_{\text{Random Releases},s} \tag{2}$$

The annual release frequency of the largest release size (100%) is due to both random leaks (see Section 2.1.1) and other releases (i.e., dispenser failures, see Section 2.1.4), as shown in Equation 3 [3].

$$f_{\text{Release},100\%} = f_{\text{Random Releases},100\%} + f_{\text{Other Releases}} \tag{3}$$

2.1.1. Frequency of Random Leaks

The annual frequency of random leaks is obtained for each release size using a fault tree [14]. These fault trees are implemented in HyRAM+ to combine individual component leak frequencies into an overall system leak frequency for each leak size. As an example, the fault tree for random leaks for leak size 0.01% is shown in Figure 2-1. The fault trees for random leaks for all other leak sizes are analogous.

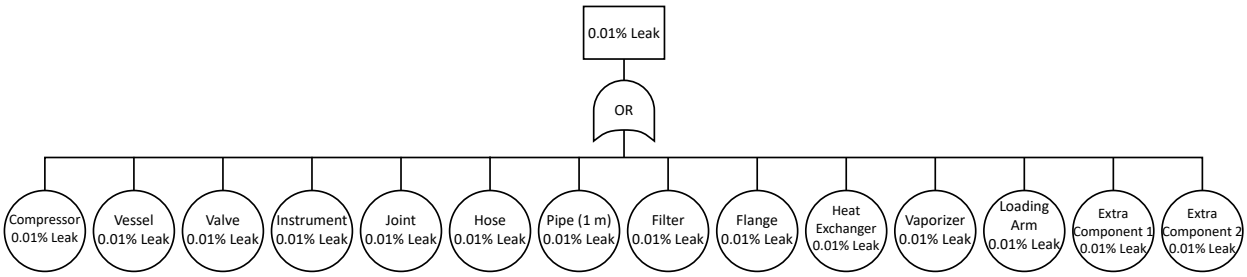

Figure 2-1 Fault tree for random leaks of size 0.01% from components.

The annual frequency of random leaks ($f_{\text{Random Releases},s}$) for a leak size s is calculated using Equation 4 by combining the individual component leak frequencies for all the components in the system of interest, where N_c is the number of components of a given type and $f_{\text{Leak}_{c,s}}$ is the annual leak frequency of leak size s for component c [3]. The component counts (N_c) and component leak frequencies ($f_{\text{Leak},c,s}$) are all user inputs, and the default values are given in Sections 2.1.2 and 2.1.3, respectively.

$$f_{\text{Random Releases},s} = \sum_{c} N_c f_{\text{Leak},c,s} \tag{4}$$

This implementation assumes that the causes in the fault tree (leaks) are mutually exclusive; this is because a hydrogen leak in a system can result in a shutdown of the system itself, thereby precluding other releases[2].

The available component types are Vessels (Cylinders/Tanks), Compressors, Flanges, Hoses, Joints, Pipes[3], Valves, Filters, Instruments, Heat Exchangers, Loading Arms, Vaporizers, Extra Component #1, and Extra Component #2 [14].

2.1.2. Default Component Counts

Default component count values are provided as a way to enable exploration of the software and should be modified by users to represent their system of interest. Default component counts are informed by systems found in the literature, and are shown in Table 2-1 [9].

[2]While simultaneous releases are still possible, depending on how quickly a system shutdown can occur, treating the events as mutually exclusive will lead to a higher (and therefore more conservative) leak frequency compared to treating leak events as independent.

[3]The "Pipes" component type is per-meter of pipe; so if a system has 15 m worth of piping, then the "number" of components for that type is 15. By contrast, the "Hoses" component type is specified as per-hose, not per-length.

Table 2-1 Default component counts for different fuels types.

Component	Gaseous Hydrogen	Liquid Hydrogen	Gaseous Methane	Liquid Methane	Propane
Compressors	1	-	1	-	1
Vessels	2	1	2	1	1
Filters	3	-	3	-	2
Flanges	-	8	-	8	8
Hoses	1	1	1	1	1
Joints	43	-	43	-	-
Pipes	30	30	30	30	30
Valves	7	44	7	44	44
Instruments	5	-	5	-	-
Heat Exchangers	-	-	1	1	-

Default component counts for gaseous hydrogen are based upon the fork lift fueling system specified in Groth et al. [17] with a compressor added based on the judgment that this would be necessary for the system [9]. Default component counts for liquid hydrogen systems come from a liquid hydrogen bulk supply system specified within CGA P-28 2014 [18], but a hose and increased length of pipe were also included based on engineering judgment [9]. Gaseous methane and blends utilize the default component counts for gaseous hydrogen, while liquid methane and propane use the default component counts for liquid hydrogen [9]. Whenever a default component leak frequency is not specified for a fuel type, due to lack of data, then the default component count for that component is zero. A heat exchanger was added to the gaseous and liquid methane default component counts due to default leak frequencies for that component being available for those fuels; a compressor was similarly added for propane [9].

2.1.3. Default Component Leak Frequencies

In HyRAM+, the annual frequency of a random leak ($f_{\text{Leak},c,s}$) for component c and leak size s is assumed to be distributed as a lognormal distribution with parameters μ and σ, as noted in Equation 5 [1–4, 17]. The μ and σ parameters are obtained from fitted distributions based on the reported distribution results from each of the original sources (see below) [12].

$$f_{\text{Leak},c,s} \sim \text{Lognormal}(\mu, \sigma^2) \tag{5}$$

The geometric mean (which is equal to the median for lognormal distributions) values are used in the frequency calculations in HyRAM+ by default as a metric of central-tendency for the distribution[4] [14]. The geometric mean is calculated using Equation 6.

$$\text{median} = e^{\mu} \tag{6}$$

[4]Probabilistic sampling of leak frequencies can be used in the HyRAM+ uncertainty propagation model, see Section 2.6.

The default values for compressed hydrogen are based on generic system leak frequencies and data from compressed hydrogen systems developed by LaChance et al. [19] and updated by both Groth et al. [17] and Glover et al. [20]. For liquid hydrogen, leak frequencies are determined using gaseous hydrogen and liquefied natural gas data as described by Brooks et al. [21]. For compressed methane, values from the analysis by Brooks et al. are used [22]. For liquid methane, the analysis described by Mulcahy et al. [23] is used. For propane, values are estimated by Brooks and Ehrhart [24] based on generic and liquid propane gas data. The leak frequency parameters for the "filter" component are updated for gaseous hydrogen, gaseous methane, and propane from the values in Brooks et al. [25].

There are two extra components (Extra Component #1 and Extra Component #2) which might not fall into the other component type categories [14]. The intention is that users can specify a custom leak frequency distribution for these components while still keeping the leak frequency distributions for the other components. These extra component leak frequencies are meant to be set by the user.

For each component for which there is no data for a specific fuel, the mean and median leak frequencies are set to infinity, with μ and σ set to 999 to achieve this effect [12]. If a user has data for these components for a specific fuel, they can be updated. If a user does not have specific information for these components for the specific fuel of interest, leak frequency distribution parameters for another fuel or another component could be used as a proxy. By making the default median frequency infinity, the risk metric will result in a value of infinity if one of these components is included in the system without leak frequency data, thereby alerting the user [12].

The default leak frequency distributions for each component are shown in Figures 2-2–2-4, and the default parameters and median values for the distributions are listed in Table 2-2.

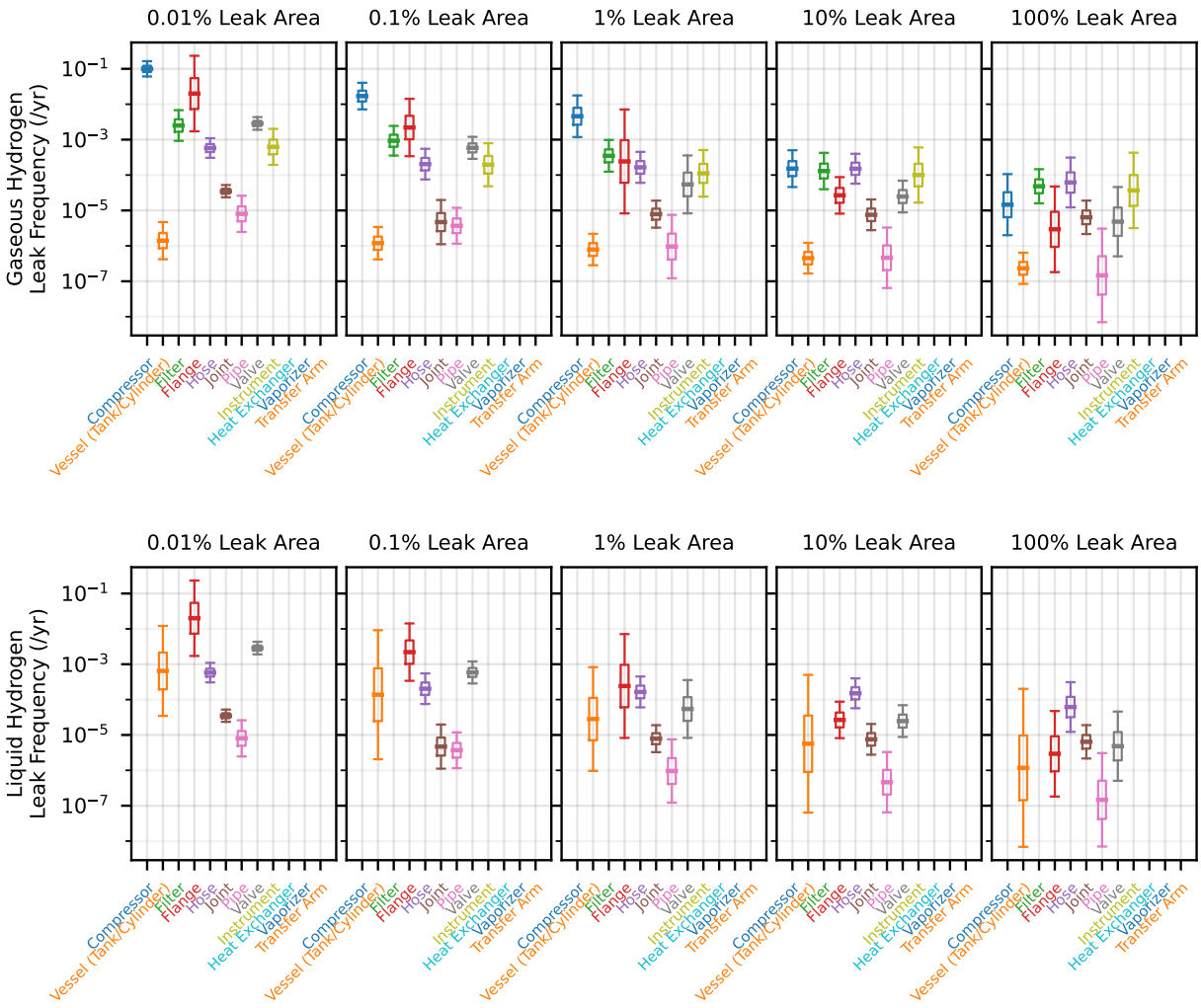

Figure 2-2 Box and whisker plots of gaseous hydrogen (top) and liquid hydrogen (bottom) leak frequencies for the different components and each leak size. The thick central line is the median leak frequency, the boxes show the 25th and 75th percentiles of the distribution and the whiskers show the 5th and 95th percentiles.

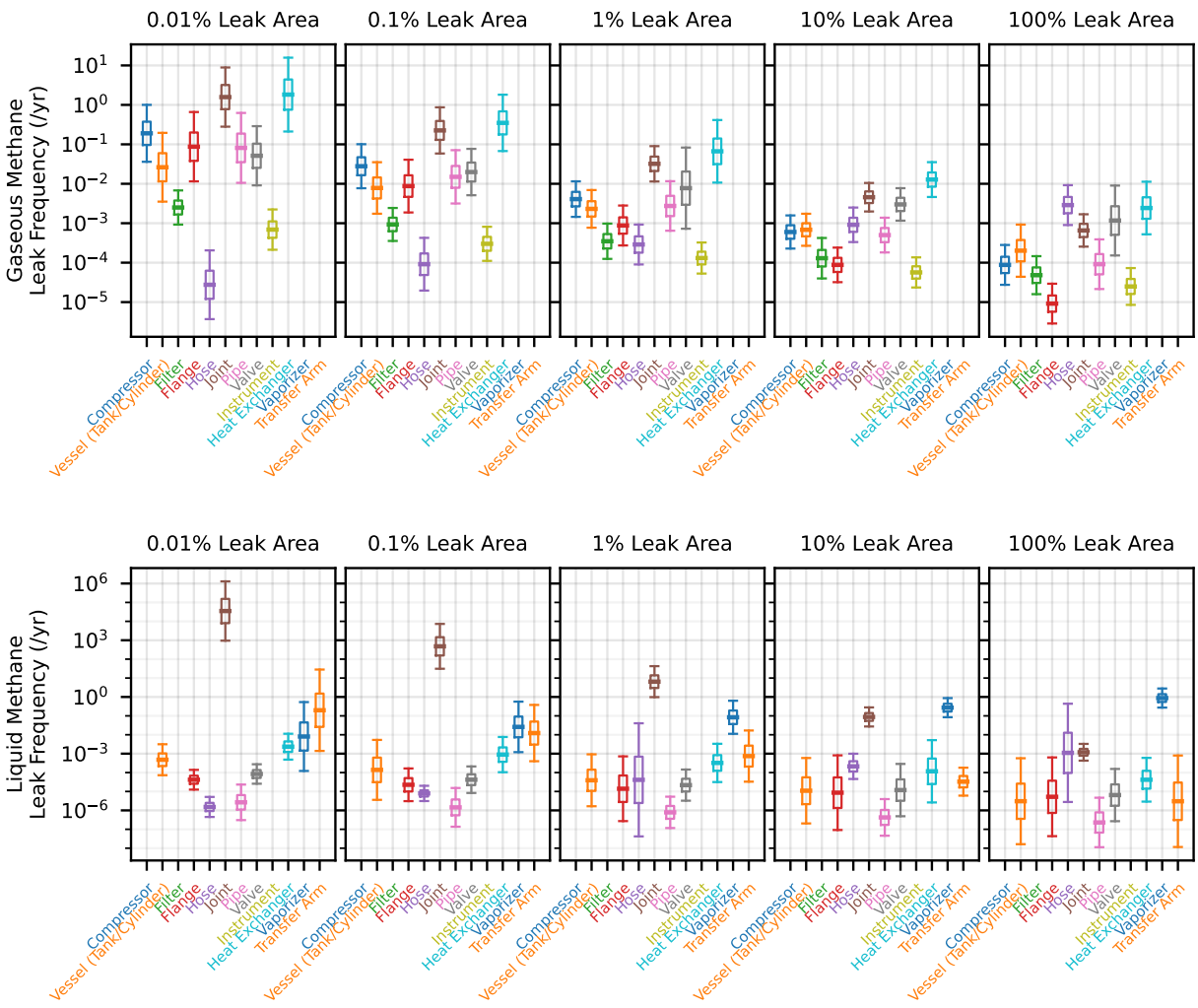

Figure 2-3 Box and whisker plots of gaseous methane (top) and liquid methane (bottom) leak frequencies for the different components and each leak size. The thick central line is the median leak frequency, the boxes show the 25th and 75th percentiles of the distribution and the whiskers show the 5th and 95th percentiles.

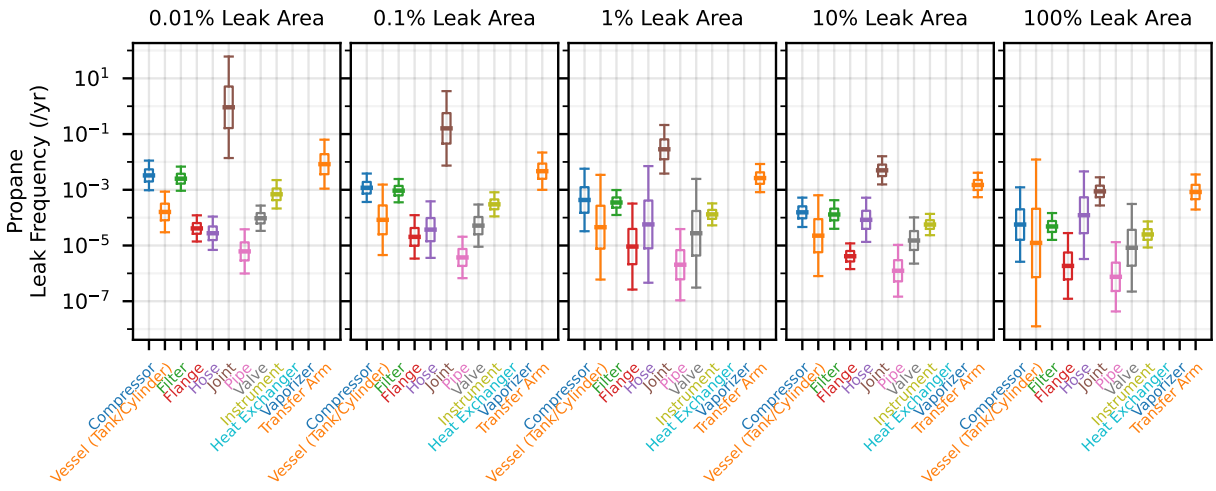

Figure 2-4 Box and whisker plot of propane (same default values for both gaseous and liquid) leak frequencies for the different components and each leak size. The thick central line is the median leak frequency, the boxes show the 25th and 75th percentiles of the distribution and the whiskers show the 5th and 95th percentiles.

Table 2-2 Default parameters for frequency of random leaks for individual components.

Component	Leak Size	Gaseous Hydrogen			Liquid Hydrogen			Gaseous Methane			Liquid Methane			Propane		
		μ	σ	median	μ	σ	median	μ	σ	median	μ	σ	median	μ	σ	median
Compressor	0.01%	-2.3	0.3	1.0×10^{-1}	999	999	∞	-1.7	1.0	1.9×10^{-1}	999	999	∞	-5.7	0.7	3.3×10^{-3}
	0.1%	-4.1	0.5	1.7×10^{-2}	999	999	∞	-3.6	0.8	2.8×10^{-2}	999	999	∞	-6.7	0.7	1.2×10^{-3}
	1%	-5.4	0.8	4.6×10^{-3}	999	999	∞	-5.5	0.6	4.1×10^{-3}	999	999	∞	-7.8	1.6	4.3×10^{-4}
	10%	-8.8	0.7	1.5×10^{-4}	999	999	∞	-7.4	0.6	6.0×10^{-4}	999	999	∞	-8.8	0.7	1.6×10^{-4}
	100%	-11.1	1.2	1.5×10^{-5}	999	999	∞	-9.3	0.7	8.8×10^{-5}	999	999	∞	-9.8	1.9	5.7×10^{-5}
Vessel (Tank/Cylinder)	0.01%	-13.5	0.7	1.4×10^{-6}	-7.3	1.8	6.5×10^{-4}	-3.6	1.2	2.6×10^{-2}	-7.6	1.1	4.8×10^{-4}	-8.7	1.0	1.6×10^{-4}
	0.1%	-13.6	0.6	1.2×10^{-6}	-8.9	2.6	1.4×10^{-4}	-4.8	0.9	7.8×10^{-3}	-8.9	2.2	1.4×10^{-4}	-9.4	1.8	8.4×10^{-5}
	1%	-14.1	0.6	7.9×10^{-7}	-10.5	2.1	2.8×10^{-5}	-6.1	0.7	2.3×10^{-3}	-10.1	1.9	3.9×10^{-5}	-10.0	2.6	4.5×10^{-5}
	10%	-14.6	0.6	4.5×10^{-7}	-12.1	2.7	5.7×10^{-6}	-7.3	0.6	6.8×10^{-4}	-11.4	2.4	1.1×10^{-5}	-10.7	2.0	2.3×10^{-5}
	100%	-15.3	0.6	2.3×10^{-7}	-13.7	3.1	1.2×10^{-6}	-8.5	0.9	2.0×10^{-4}	-12.7	3.2	3.1×10^{-6}	-11.3	4.2	1.2×10^{-5}
Filter	0.01%	-6.0	0.6	2.5×10^{-3}	999	999	∞	-6.0	0.6	2.5×10^{-3}	999	999	∞	-6.0	0.6	2.5×10^{-3}
	0.1%	-7.0	0.6	9.3×10^{-4}	999	999	∞	-7.0	0.6	9.3×10^{-4}	999	999	∞	-7.0	0.6	9.3×10^{-4}
	1%	-8.0	0.6	3.5×10^{-4}	999	999	∞	-8.0	0.6	3.5×10^{-4}	999	999	∞	-8.0	0.6	3.5×10^{-4}
	10%	-8.9	0.7	1.3×10^{-4}	999	999	∞	-8.9	0.7	1.3×10^{-4}	999	999	∞	-8.9	0.7	1.3×10^{-4}
	100%	-9.9	0.7	4.8×10^{-5}	999	999	∞	-9.9	0.7	4.8×10^{-5}	999	999	∞	-9.9	0.7	4.8×10^{-5}
Flange	0.01%	-3.9	1.5	2.0×10^{-2}	-3.9	1.5	2.0×10^{-2}	-2.4	1.2	8.7×10^{-2}	-10.1	0.7	4.2×10^{-5}	-10.1	0.7	4.1×10^{-5}
	0.1%	-6.1	1.1	2.2×10^{-3}	-6.1	1.1	2.2×10^{-3}	-4.7	0.9	8.7×10^{-3}	-10.7	1.2	2.3×10^{-5}	-10.8	1.1	2.0×10^{-5}
	1%	-8.3	2.1	2.4×10^{-4}	-8.3	2.1	2.4×10^{-4}	-7.0	0.7	8.8×10^{-4}	-11.2	2.4	1.4×10^{-5}	-11.6	2.2	9.2×10^{-6}
	10%	-10.5	0.7	2.7×10^{-5}	-10.5	0.7	2.7×10^{-5}	-9.3	0.6	8.8×10^{-5}	-11.7	2.8	8.6×10^{-6}	-12.4	0.6	4.1×10^{-6}
	100%	-12.7	1.7	2.9×10^{-6}	-12.7	1.7	2.9×10^{-6}	-11.6	0.7	9.2×10^{-6}	-12.2	2.9	5.2×10^{-6}	-13.2	1.6	1.9×10^{-6}
Hose	0.01%	-7.5	0.4	5.8×10^{-4}	-7.5	0.4	5.8×10^{-4}	-10.5	1.2	2.8×10^{-5}	-13.4	0.7	1.5×10^{-6}	-10.5	0.8	2.8×10^{-5}
	0.1%	-8.5	0.6	2.0×10^{-4}	-8.5	0.6	2.0×10^{-4}	-9.3	0.9	9.1×10^{-5}	-11.7	0.6	7.9×10^{-6}	-10.2	1.4	3.7×10^{-5}
	1%	-8.7	0.6	1.6×10^{-4}	-8.7	0.6	1.6×10^{-4}	-8.2	0.7	2.9×10^{-4}	-10.1	4.2	4.1×10^{-5}	-9.8	2.9	5.7×10^{-5}
	10%	-8.8	0.6	1.5×10^{-4}	-8.8	0.6	1.5×10^{-4}	-7.0	0.6	9.1×10^{-4}	-8.5	0.9	2.1×10^{-4}	-9.4	1.1	8.4×10^{-5}
	100%	-9.7	1.0	6.2×10^{-5}	-9.7	1.0	6.2×10^{-5}	-5.8	0.7	2.9×10^{-3}	-6.8	3.6	1.1×10^{-3}	-9.0	2.2	1.2×10^{-4}
Joint	0.01%	-10.3	0.2	3.5×10^{-5}	-10.3	0.2	3.5×10^{-5}	0.5	1.1	1.6×10^{0}	10.5	2.2	3.5×10^{4}	-0.1	2.5	9.2×10^{-1}
	0.1%	-12.3	0.9	4.7×10^{-6}	-12.3	0.9	4.7×10^{-6}	-1.5	0.8	2.3×10^{-1}	6.2	1.7	4.8×10^{2}	-1.8	1.9	1.6×10^{-1}
	1%	-11.8	0.5	7.9×10^{-6}	-11.8	0.5	7.9×10^{-6}	-3.4	0.6	3.2×10^{-2}	1.9	1.1	6.5×10^{0}	-3.6	1.2	2.8×10^{-2}
	10%	-11.8	0.6	7.5×10^{-6}	-11.8	0.6	7.5×10^{-6}	-5.4	0.5	4.6×10^{-3}	-2.4	0.7	8.8×10^{-2}	-5.3	0.7	5.0×10^{-3}
	100%	-12.0	0.7	6.4×10^{-6}	-12.0	0.7	6.4×10^{-6}	-7.3	0.6	6.6×10^{-4}	-6.7	0.6	1.2×10^{-3}	-7.0	0.7	8.8×10^{-4}
Pipe	0.01%	-11.7	0.7	8.0×10^{-6}	-11.7	0.7	8.0×10^{-6}	-2.5	1.2	8.1×10^{-2}	-12.8	1.3	2.7×10^{-6}	-12.0	1.1	6.1×10^{-6}
	0.1%	-12.5	0.7	3.7×10^{-6}	-12.5	0.7	3.7×10^{-6}	-4.2	0.9	1.5×10^{-2}	-13.4	1.4	1.4×10^{-6}	-12.5	1.0	3.7×10^{-6}
	1%	-13.9	1.3	9.6×10^{-7}	-13.9	1.3	9.6×10^{-7}	-5.9	0.9	2.7×10^{-3}	-14.1	1.2	7.9×10^{-7}	-13.1	1.8	2.0×10^{-6}
	10%	-14.6	1.2	4.6×10^{-7}	-14.6	1.2	4.6×10^{-7}	-7.6	0.6	5.0×10^{-4}	-14.7	1.4	4.2×10^{-7}	-13.6	1.3	1.2×10^{-6}
	100%	-15.7	1.8	1.5×10^{-7}	-15.7	1.8	1.5×10^{-7}	-9.3	0.9	9.1×10^{-5}	-15.3	1.8	2.3×10^{-7}	-14.1	1.7	7.5×10^{-7}
Valve	0.01%	-5.9	0.2	2.9×10^{-3}	-5.9	0.2	2.9×10^{-3}	-3.0	1.1	5.1×10^{-2}	-9.4	0.7	8.4×10^{-5}	-9.3	0.6	9.5×10^{-5}
	0.1%	-7.4	0.4	5.9×10^{-4}	-7.4	0.4	5.9×10^{-4}	-3.9	0.8	2.0×10^{-2}	-10.1	1.0	4.2×10^{-5}	-9.9	1.1	5.2×10^{-5}
	1%	-9.8	1.1	5.4×10^{-5}	-9.8	1.1	5.4×10^{-5}	-4.9	1.4	7.8×10^{-3}	-10.7	1.2	2.2×10^{-5}	-10.5	2.7	2.8×10^{-5}
	10%	-10.6	0.6	2.5×10^{-5}	-10.6	0.6	2.5×10^{-5}	-5.8	0.6	3.0×10^{-3}	-11.3	1.9	1.2×10^{-5}	-11.1	1.2	1.5×10^{-5}
	100%	-12.2	1.4	4.8×10^{-6}	-12.2	1.4	4.8×10^{-6}	-6.8	1.2	1.2×10^{-3}	-11.9	1.9	6.5×10^{-6}	-11.7	2.2	8.3×10^{-6}
Instrument	0.01%	-7.4	0.7	6.2×10^{-4}	999	999	∞	-7.3	0.7	6.9×10^{-4}	999	999	∞	-7.3	0.7	6.9×10^{-4}
	0.1%	-8.5	0.8	2.0×10^{-4}	999	999	∞	-8.1	0.6	3.0×10^{-4}	999	999	∞	-8.1	0.6	3.0×10^{-4}
	1%	-9.1	0.9	1.1×10^{-4}	999	999	∞	-8.9	0.6	1.3×10^{-4}	999	999	∞	-8.9	0.6	1.3×10^{-4}
	10%	-9.2	1.1	1.0×10^{-4}	999	999	∞	-9.8	0.5	5.7×10^{-5}	999	999	∞	-9.8	0.5	5.7×10^{-5}
	100%	-10.2	1.5	3.7×10^{-5}	999	999	∞	-10.6	0.7	2.5×10^{-5}	999	999	∞	-10.6	0.7	2.5×10^{-5}
Heat Exchanger	0.01%	999	999	∞	999	999	∞	0.6	1.3	1.8×10^{0}	-6.1	1.0	2.3×10^{-3}	999	999	∞
	0.1%	999	999	∞	999	999	∞	-1.1	1.0	3.5×10^{-1}	-7.0	1.3	8.9×10^{-4}	999	999	∞
	1%	999	999	∞	999	999	∞	-2.7	1.1	6.7×10^{-2}	-8.0	1.4	3.2×10^{-4}	999	999	∞
	10%	999	999	∞	999	999	∞	-4.4	0.6	1.3×10^{-2}	-9.1	2.3	1.2×10^{-4}	999	999	∞
	100%	999	999	∞	999	999	∞	-6.0	0.9	2.4×10^{-3}	-10.1	1.6	4.2×10^{-5}	999	999	∞
Vaporizer	0.01%	999	999	∞	999	999	∞	999	999	∞	-4.8	2.5	8.1×10^{-3}	999	999	∞
	0.1%	999	999	∞	999	999	∞	999	999	∞	-3.6	1.9	2.6×10^{-2}	999	999	∞
	1%	999	999	∞	999	999	∞	999	999	∞	-2.5	1.2	8.4×10^{-2}	999	999	∞
	10%	999	999	∞	999	999	∞	999	999	∞	-1.3	0.7	2.7×10^{-1}	999	999	∞
	100%	999	999	∞	999	999	∞	999	999	∞	-0.1	0.7	8.8×10^{-1}	999	999	∞
Transfer Arm	0.01%	999	999	∞	999	999	∞	999	999	∞	-1.6	3.0	2.0×10^{-1}	-4.8	1.2	8.3×10^{-3}
	0.1%	999	999	∞	999	999	∞	999	999	∞	-4.4	2.1	1.2×10^{-2}	-5.4	0.9	4.7×10^{-3}
	1%	999	999	∞	999	999	∞	999	999	∞	-7.2	1.9	7.5×10^{-4}	-5.9	0.7	2.6×10^{-3}
	10%	999	999	∞	999	999	∞	999	999	∞	-10.3	1.0	3.3×10^{-5}	-6.5	0.6	1.5×10^{-3}
	100%	999	999	∞	999	999	∞	999	999	∞	-12.7	3.4	3.0×10^{-6}	-7.1	0.9	8.3×10^{-4}

2.1.4. Frequency of Dispenser Releases

The annual frequency of other releases ($f_{\text{Other Releases}}$) deals with failures that can happen at a dispenser, rather than random leaks from individual components [14, 17]. The probability of an accident can be high for several reasons: fueling typically involves direct human interaction to operate the fueling dispenser, connections are temporary rather than hard-plumbed lines, and connections can be inadvertently broken because the vehicle is not a permanent part of the system. On the other hand, releases from fueling can only occur when fueling occurs, and so different systems that involve different numbers of fueling events can be impacted by these releases to varying degrees. It is assumed that a dispenser failure would result in a large release of fuel, and so this frequency is only used in the largest (100%) leak size.

The annual frequency of other releases ($f_{\text{Other Releases}}$) is calculated using Equation 7, in which $f_{\text{Fueling Demands}}$ is the annual frequency of fueling demands (i.e., the number of times a dispenser is used to refuel a vehicle in a year) and $p_{\text{Dispenser Releases}}$ is the probability of a release from a dispenser during fueling [14]. This implementation assumes that the causes in the fault tree are mutually exclusive; this is because a hydrogen leak in a system can result in a shutdown of the system itself, thereby precluding other releases[5].

$$f_{\text{Other Releases}} = f_{\text{Fueling Demands}} \times p_{\text{Dispenser Releases}} \tag{7}$$

The annual frequency of fueling demands ($f_{\text{Fueling Demands}}$) is given by Equation 8, where N_{Vehicles} is the number of vehicles at the facility, $N_{\text{Fuelings per Day}}$ is the average number of times each vehicle is fueled per day, and $N_{\text{Operating Days per Year}}$ is the number of operating days in a year [14].

$$f_{\text{Fueling Demands}} = N_{\text{Vehicles}} \times N_{\text{Fuelings per Day}} \times N_{\text{Operating Days per Year}} \tag{8}$$

Dispenser failures are categorized in HyRAM+ as Accidents (in which the vehicle tank overpressurizes or a drive-off occurs) or Shutdown Failures (in which the system fails to shut down after a release from the nozzle) [14]. The probability for these types of releases are estimated using a fault tree as shown in Figure 2-5.

[5] While simultaneous releases are still possible, depending on how quickly a system shutdown can occur, treating the events as mutually exclusive will lead to a higher (and therefore more conservative) release probability compared to treating leak events as independent.

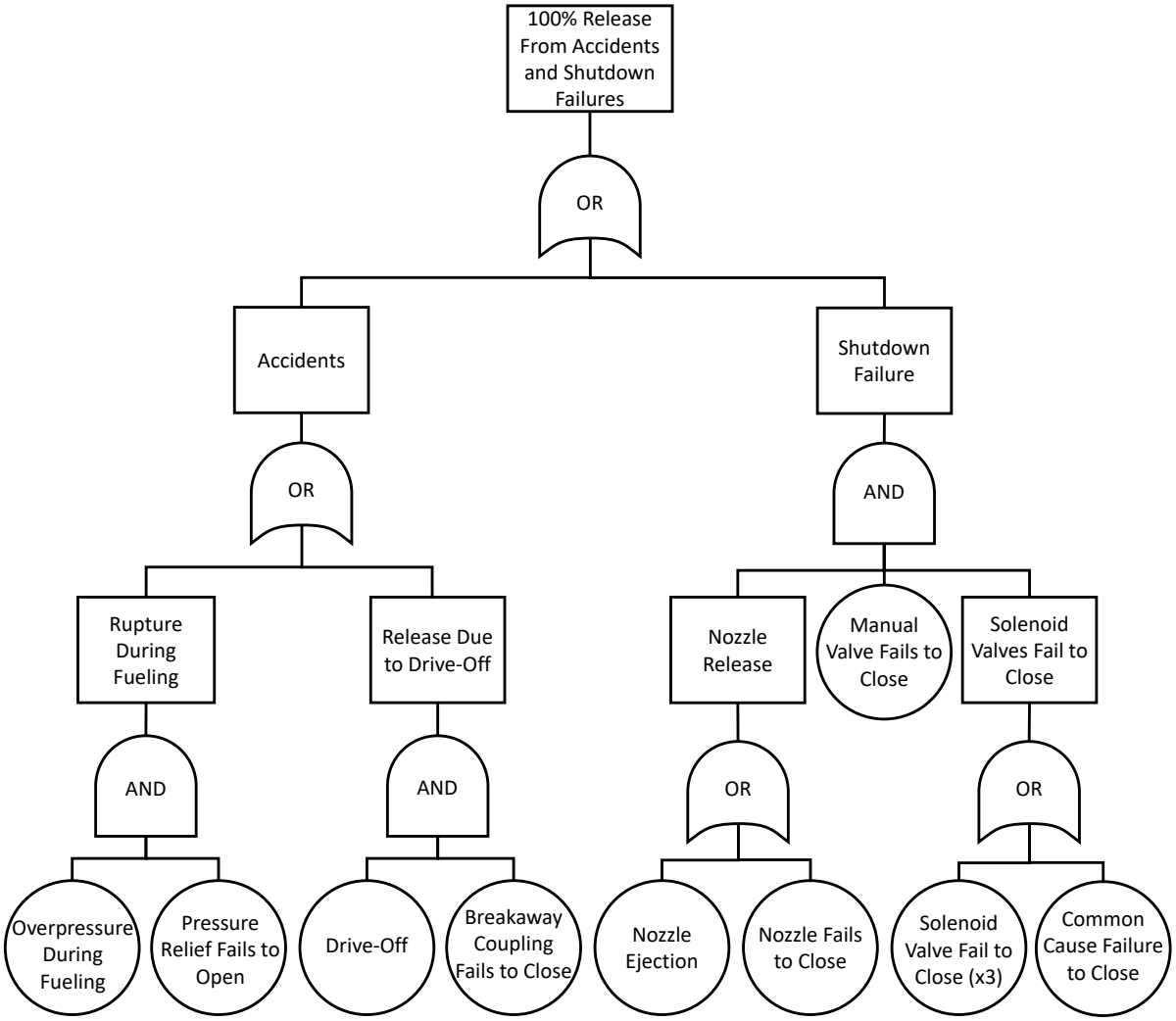

Figure 2-5 Fault tree for Other Releases from a dispenser [14].

The probability of a release from a dispenser during fueling ($p_{\text{Dispenser Releases}}$) is given by Equation 9, where $p_{\text{Accidents}}$ is the probability of an accident during fueling and $p_{\text{Shutdown Failure}}$ is the probability of a shutdown failure during fueling [14].

$$p_{\text{Dispenser Releases}} = p_{\text{Accidents}} + p_{\text{Shutdown Failure}} \tag{9}$$

The probability of an accident during fueling ($p_{\text{Accidents}}$) is given by Equation 10, where $p_{\text{Rupture During Fueling}}$ is the probability of a rupture that occurs during fueling and $p_{\text{Release Due to Drive-Off}}$ is the probability of a release occurring due to a vehicle drive-off [14].

$$p_{\text{Accidents}} = p_{\text{Rupture During Fueling}} + p_{\text{Release Due to Drive-Off}} \tag{10}$$

The probability of a rupture during fueling is given by Equation 11, in which $p_{\text{Overpressure During Fueling}}$ is the probability of an overpressure occurring during fueling (e.g., the

dispenser over-fills the vehicle tank) and $p_{\text{PRD FTO}}$ is the probability of the dispenser pressure relief device failing to open on demand [14].

$$p_{\text{Rupture During Fueling}} = p_{\text{Overpressure During Fueling}} \times p_{\text{PRD FTO}} \tag{11}$$

The probability of a release occurring due to a vehicle drive-off ($p_{\text{Release Due to DriveOff}}$) is given by Equation 12, where p_{DriveOff} is the probability of a vehicle driving off while still attached to the dispenser during fueling and $p_{\text{Breakaway FTC}}$ is the probability of the breakaway coupling failing to close on demand [14].

$$p_{\text{Release Due to DriveOff}} = p_{\text{DriveOff}} \times p_{\text{Breakaway FTC}} \tag{12}$$

The probability of a shutdown failure during fueling ($p_{\text{Shutdown Failure}}$) is given by Equation 13, where $p_{\text{Nozzle Release}}$ is the probability of the dispensing nozzle releasing fuel, $p_{\text{Manual Valve FTC}}$ is the probability of the manual shutoff valve failing to close on demand, and $p_{\text{Solenoid Valves FTC}}$ is the probability of the automated solenoid valves on the dispenser failing to close on demand [14].

$$p_{\text{Shutdown Failure}} = p_{\text{Nozzle Release}} \times p_{\text{Manual Valve FTC}} \times p_{\text{Solenoid Valves FTC}} \tag{13}$$

The probability of the dispensing nozzle releasing fuel ($p_{\text{Nozzle Release}}$) is given by Equation 14, in which $p_{\text{Nozzle Ejection}}$ is the probability of the dispenser nozzle being ejected during fueling, and $p_{\text{Nozzle FTC}}$ is the probability of the dispenser nozzle failing to close on demand [14].

$$p_{\text{Nozzle Release}} = p_{\text{Nozzle Ejection}} + p_{\text{Nozzle FTC}} \tag{14}$$

The probability of the automated solenoid valves on the dispenser failing to close on demand ($p_{\text{Solenoid Valves FTC}}$) is given by Equation 15, where $p_{\text{Solenoid Valve FTC}}$ is the probability of any one automated solenoid valve failing to close on demand and $p_{\text{Common Cause FTC}}$ is the probability of something causing all of the solenoid valves to fail to close on demand (e.g., loss of connection to sensors) [14].

$$p_{\text{Solenoid Valves FTC}} = [p_{\text{Solenoid Valve FTC}}]^3 + p_{\text{Common Cause FTC}} \tag{15}$$

It should be noted that this fault tree implementation assumes that there are 3 solenoid valves and that all of them need to fail in order for fuel to be released; thus, the probability for any single valve failing is cubed.

The probabilities $p_{\text{Overpressure During Fueling}}$, $p_{\text{PRD FTO}}$, p_{DriveOff}, $p_{\text{Breakaway FTC}}$, $p_{\text{Manual Valve FTC}}$, $p_{\text{Nozzle Ejection}}$, $p_{\text{Nozzle FTC}}$, $p_{\text{Solenoid Valve FTC}}$, and $p_{\text{Common Cause FTC}}$ can each be specified as a specific expected value from 0.0 to 1.0, or can be specified as a probability distribution such as beta or lognormal distributions [14]. If a probability distribution is specified, the mean (or median for a lognormal distribution) value will be calculated and used in the above calculations. Default values for these probabilities are given in Section 2.1.5.

Any of the probabilities in this section can be used to estimate an annual frequency of any of the events in question. This can be done by multiplying the probability for event of interest A (p_A) by the annual number of fueling demands ($f_{\text{Fueling Demands}}$), as shown in Equation 16 [14].

$$f_A = p_A \times f_{\text{Fueling Demands}} \tag{16}$$

2.1.5. Default Dispenser Failure Probabilities

The default dispenser failure probabilities in HyRAM+ were estimated from generic data from the offshore oil, process chemical, and nuclear power industries as part of a risk assessment for indoor refueling of hydrogen-powered forklifts [17]. Table 2-3 shows the default probability distributions and parameters for various types of component-specific dispenser failures and Table 2-4 shows the default accident occurrence probability distributions and parameters for different types of accidents for dispensers that are described in Section 2.1.4.

Table 2-3 Default probability distributions and parameters for dispenser failure.

Component	Failure Mode	Variable	Distribution	Parameters
Nozzle	Pop-off	$p_{\text{Nozzle Ejection}}$	Beta (α, β)	$\alpha = 0.5$ $\beta = 610415.5$
Nozzle	Failure to close	$p_{\text{Nozzle FTC}}$	Expected value	0.002
Breakaway coupling	Failure to close	$p_{\text{Breakaway FTC}}$	Beta (α, β)	$\alpha = 0.5$ $\beta = 5031$
Pressure relief valve	Failure to open	$p_{\text{PRD FTO}}$	Lognormal (μ, σ^2)	$\mu = -11.74$ $\sigma = 0.67$
Manual valve	Failure to close	$p_{\text{Manual Valve FTC}}$	Expected value	0.001
Solenoid valve	Failure to close	$p_{\text{Solenoid Valve FTC}}$	Expected value	0.002
Solenoid valves	Common cause failure	$p_{\text{Common Cause FTC}}$	Expected value	1.28×10^{-4}

Table 2-4 Default probability distributions for accident occurrence.

Accident	Variable	Distribution	Parameters
Drive-off	p_{DriveOff}	Beta (α, β)	$\alpha = 31.5$ $\beta = 610384.5$
Overpressure during fueling	$p_{\text{Overpressure During Fueling}}$	Beta (α, β)	$\alpha = 3.5$ $\beta = 310289.5$

See Equation 6 for the calculation of the geometric mean (median) for a lognormal distribution. For a beta distribution with parameters α and β, the arithmetic mean is calculated using Equation 17[6].

$$\text{mean} = \frac{\alpha}{\alpha + \beta} \tag{17}$$

[6]Probabilistic sampling of dispenser failure probabilities can be used in the HyRAM+ uncertainty propagation model, see Section 2.6.

The default number of vehicles that use the dispenser (N_{Vehicles}) is 20, each with 2 fuelings per day ($N_{\text{Fuelings per Day}}$), and the default number of vehicle operating days per year ($N_{\text{Operating Days per Year}}$) is 250. This results in 10,000 annual fueling demands by default ($f_{\text{Fueling Demands}}$, see Equation 8).

2.2. Outcome Likelihood of a Release

A release of a flammable fuel could lead to several possible hazards [2–4]. Currently, HyRAM+ calculates harm from thermal effects of jet fires (for immediate ignition) and overpressure (for delayed ignition). A release of a liquid fuel (e.g., liquid hydrogen or liquid natural gas) may also form a pool on the ground, but this is currently not considered in HyRAM+, nor are the thermal effects from the cold temperatures of these cryogenic liquid fuels. The likelihood of potentially harmful scenarios is estimated using an event sequence diagram[7] for release of a flammable fuel, shown in Figure 2-6.

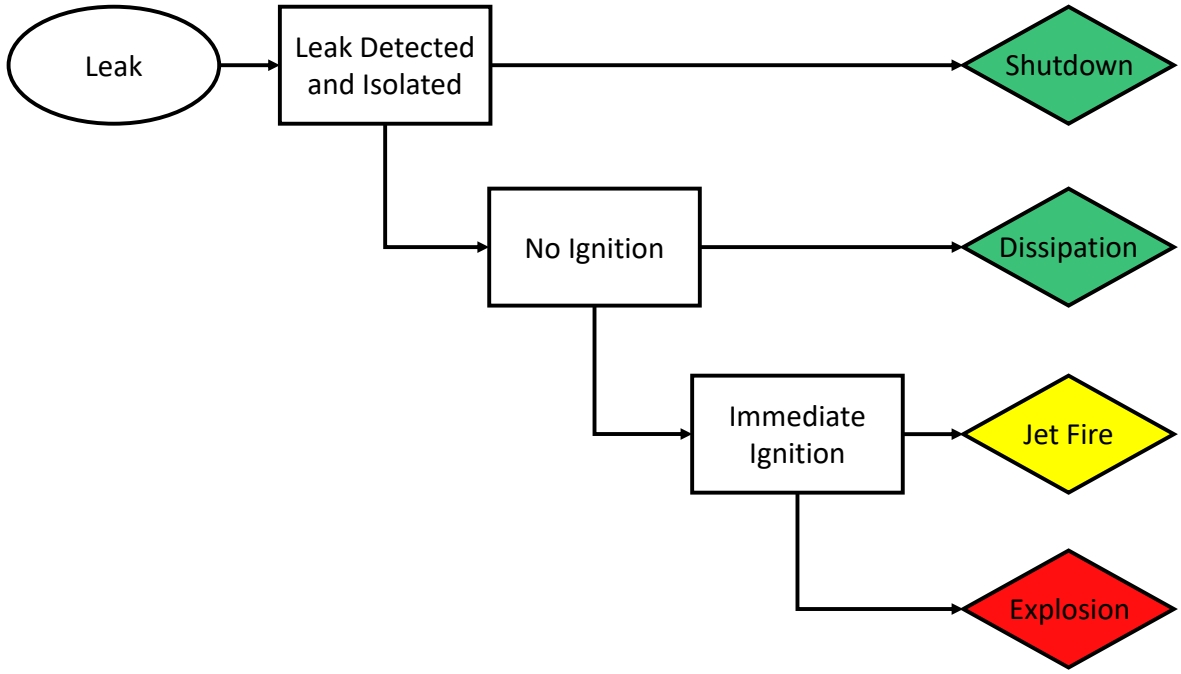

Figure 2-6 Event sequence diagram used by HyRAM+ for flammable gas releases (adapted from [14]).

The probability of the first outcome, Shutdown, is given by Equation 18, in which p_{Shutdown} is the probability of the Shutdown outcome given a leak and p_{Isolate} is the probability of detecting and isolating a release (leak) before ignition. The probability of detecting and isolating a release (leak) before ignition (p_{Isolate}) is a user input, and the default value is given in Section 2.2.1.

$$p_{\text{Shutdown}} = p_{\text{Isolate}} \tag{18}$$

[7] Also called an event tree.

The probability of the second outcome, Dissipation, is given by Equation 19, in which $p_{\text{Dissipation}}$ is the probability of the Dissipation outcome given a leak and $p_{\text{NoIgnition}}$ is the probability of ignition not occurring for a given release (leak). This includes the probability of failing to detect and isolate a release (leak) without ignition, as shown in the event tree (Figure 2-6), which is the $(1 - p_{\text{Isolate}})$ term in Equation 19.

$$p_{\text{Dissipation}} = (1 - p_{\text{Isolate}})\, p_{\text{NoIgnition}} \tag{19}$$

The probability of ignition not occurring for a given release ($p_{\text{NoIgnition}}$) is the complementary probability of the total probability of ignition given a release (p_{Ignition}), as shown in Equation 20.

$$p_{\text{NoIgnition}} = 1 - p_{\text{Ignition}} \tag{20}$$

The total probability of ignition given a release (p_{Ignition}) is a combination of the probability of immediate ignition given a release ($p_{\text{ImmediateIgnition}}$) and the probability of delayed ignition given a release ($p_{\text{DelayedIgnition}}$), as shown in Equation 21. These equations are written in this way to utilize immediate and delayed ignition probabilities that are each conditional to a leak occurring as user inputs. The default values for these ignition probability inputs ($p_{\text{ImmediateIgnition}}$ and $p_{\text{DelayedIgnition}}$) are given in Section 2.2.2.

$$p_{\text{Ignition}} = p_{\text{ImmediateIgnition}} + p_{\text{DelayedIgnition}} \tag{21}$$

The probability of the third outcome, Jet Fire, is given by Equation 22, in which p_{JetFire} is the probability of the Jet Fire outcome given a leak and $p_{\text{Immediate}}$ is the probability of immediate ignition given that ignition has occurred. This includes the probability of failing to detect and isolate a release (leak) without ignition, as well as the probability of ignition occurring.

$$p_{\text{JetFire}} = (1 - p_{\text{Isolate}}) \left(1 - p_{\text{NoIgnition}}\right) p_{\text{Immediate}} \tag{22}$$

The probability of immediate ignition given that ignition has occurred ($p_{\text{Immediate}}$) can be calculated from the probability of immediate ignition given a release ($p_{\text{ImmediateIgnition}}$) and the total probability of ignition given a release (p_{Ignition}), as shown in Equation 23.

$$p_{\text{Immediate}} = \frac{p_{\text{ImmediateIgnition}}}{p_{\text{Ignition}}} \tag{23}$$

The probability of the fourth and final outcome, Explosion, is given by Equation 24, in which $p_{\text{Explosion}}$ is the probability of the Explosion outcome given a leak. This includes the probability of detecting and isolating a release (leak) before ignition not occurring, the probability of ignition occurring, and the probability of immediate ignition not occurring.

$$p_{\text{Explosion}} = (1 - p_{\text{Isolate}}) \left(1 - p_{\text{NoIgnition}}\right) (1 - p_{\text{Immediate}}) \tag{24}$$

As with any such event sequence diagram, the probabilities of all outcomes (o) given that a release has occurred (Equations 18–24) sum to 1, as shown in Equation 25.

$$\sum_{o} p_o = 1 = p_{\text{Shutdown}} + p_{\text{Dissipation}} + p_{\text{JetFire}} + p_{\text{Explosion}} \tag{25}$$

The annual frequency of any of these outcomes ($f_{s,o}$ for leak size s and outcome o, see Equations 18–24) can be obtained by multiplying the annual frequency of a leak of a given size ($f_{\text{Release},s}$ for leak size s, see Section 2.1) by the probability for each outcome ($p_{s,o}$, see Equations 18–24), as shown in Equation 26.

$$f_{s,o} = f_{\text{Release},s} p_{s,o} \tag{26}$$

2.2.1. Default Detection and Isolation Probability

Successful release detection and isolation (p_{Isolate}) is assigned a default value of 0.9 [3]. This value incorporates many considerations on detection and isolation including ventilation, sensor placement, leak location, and the ability of the sensor and isolation valve to operate successfully on demand.

Note: This value can vary significantly based on a particular system setup, and so the user/analyst needs to carefully consider the particulars of the system being assessed and decide if this default value is appropriate.

2.2.2. Default Ignition Probabilities

The default values for the probability of immediate ignition given a release ($p_{\text{ImmediateIgnition}}$) and the probability of delayed ignition given a release ($p_{\text{DelayedIgnition}}$) are a function of release rate and are given in Table 2-5 [26].

Table 2-5 Default ignition probabilities for different fuels.

(a) Hydrogen

Release Rate (kg/s)	Ignition Probability	
	Immediate	Delayed
<0.125	0.008	0.004
0.125–6.25	0.053	0.027
>6.25	0.230	0.120

(b) Methane and Propane

Release Rate (kg/s)	Ignition Probability	
	Immediate	Delayed
<1	0.007	0.003
1–50	0.047	0.023
>50	0.200	0.100

2.3. Consequence Models

The consequences of a leak scenario outcome ($c_{s,o}$) can vary by both the leak size s (0.01%, 0.1%, 1%, 10%, and 100% leak sizes) and by outcome o (see Section 2.2). As HyRAM+ calculates the fatality risk, the consequences are calculated from the estimated likelihood of a fatality from each of the l occupants of the facility (see Section 2.3.1). Thus, the consequences for each leak size,

outcome, and occupant ($c_{s,o,l}$) combine to calculate the consequence for that leak size and outcome ($c_{s,o}$) as shown in Equation 27.

$$c_{s,o} = \sum_{l} c_{s,o,l} \tag{27}$$

The consequences for each of the leak scenarios are estimated by the probability of a fatality for each of the occupants in the facility, as described in the following sub-sections.

2.3.1. Facility Occupants

The harm and fatalities of interest in HyRAM+ are calculated for individual facility occupants [14, 17]. The occupant positions and number of occupants are defined by user input. For each dimension of the occupant position (x, y, z) for each occupant, the user may assign a position deterministically or may specify a probability distribution. Probability distributions are randomly sampled to assign the positions using user-specified inputs to a uniform or normal distribution. The occupant positions are all defined relative to the leak point; i.e., the leak occurs at the "origin" (0, 0, 0) and extends in the xy-plane depending on the angle of the leak, so the occupant positions (x, y, z) are based on that point of reference. The x and z coordinates are horizontal to the ground, while the y coordinate is height above the ground. The occupants are assumed not to occupy the same physical space as the leak point, and so an exclusion radius is used; if a generated occupant position is within the specified exclusion radius, that position is rejected and another position generated. By default, the exclusion radius is 0.01 m.

The occupant locations are sampled and assigned once per QRA calculation; this means that if any occupant location dimensions are specified with a probability distribution, the resulting risk value may differ between calculation runs. Instead, if occupant locations are specified deterministically for all dimensions, then the same risk value result will occur for each calculation run. A user who wants to repeat a previously specified set of determined locations can either specify those locations deterministically or use the same value for the "random seed" input, which will cause the same values to be sampled from the probability distributions.

By default, HyRAM+ includes a set of 9 occupants that are meant to provide an example of workers within a station or facility. The locations of these default occupants are assumed to be distributed with a uniform distribution in the x-direction between 1–20 m, a constant height of 0 m (i.e., same height as the leak itself), and distributed with a uniform distribution in the z-direction between 1–12 m. These default occupants are assumed to have 2,000 exposed hours per occupant per year. The number, location specifications, and exposed hours for these default occupants can be edited by the user, and additional groups with occupants with separate numbers, locations, and exposed hours can be specified by the user as well.

2.3.2. Shutdown Scenario Consequences

The scenario in which a leak is safely detected and isolated is assumed to result in no fatalities for all of the occupant positions [17], as shown in Equation 28.

$$c_{s,\text{Shutdown},l} = 0 \tag{28}$$

2.3.3. Dissipation Scenario Consequences

The scenario in which a leak dissipates and does not ignite is assumed to result in no fatalities for all of the occupant positions [17], as shown in Equation 29.

$$c_{s,\text{Dissipation},l} = 0 \tag{29}$$

2.3.4. Jet Fire Scenario Consequences

The consequences of a jet fire on facility occupants are calculated using Equation 30, in which $p_{\text{fatal},s,\text{jetfire},l}$ is the probability of a fatality from a jet fire for the leak size s and occupant location l.

$$c_{s,\text{Jetfire},l} = p_{\text{fatal},s,\text{jetfire},l} \tag{30}$$

The probability of a fatality from a jet fire is described in Section 2.4, which uses physical effect modeling as described in Section 3. Specifically, the flame model described in Section 3.4.2 and multi-point radiative heat flux model described in Section 3.4.3 are used for this scenario. These models are coupled to the developing flow models described in Section 3.2. The heat flux calculation is performed at each of the occupant locations, and the resulting values are then used to estimate the probability of a fatality at each of the occupant locations using the fatality probits in Section 2.4.1.

2.3.5. Explosion Scenario Consequences

The consequences of an explosion on facility occupants are calculated using Equation 31, in which $p_{\text{fatal},s,\text{explosion},l}$ is the probability of a fatality from an explosion for the leak size s and occupant position l.

$$c_{s,\text{Explosion},l} = p_{\text{fatal},s,\text{explosion},l} \tag{31}$$

The probability of a fatality from an explosion is described in Section 2.4, which uses physical effect modeling as described in Section 3. The unconfined overpressure model described in Section 3.4.5 is used for this scenario; this assumes that the overpressure occurs outdoors or in a large enough indoor space such that the overpressure is unconfined. The overpressure calculation is performed at each of the occupant locations, and the resulting values are then used to estimate the probability of a fatality at each of the occupant locations using the fatality probits in Section 2.4.2.

2.4. Harm and Loss Models

Probit models are used in HyRAM+ to estimate the probability of a fatality for a given harmful effect [1–4, 17]. The probability of a fatality for the probit models in HyRAM+ is given by Equation 32, which is the standard normal cumulative distribution function evaluated at Y; Y is obtained by the corresponding probit model (see Sections 2.4.1 and 2.4.2) [3, 17]. The standard normal cumulative distribution function ($\Phi(x)$) is the case in which the normal cumulative distribution function ($F(x|\mu, \sigma)$) has parameters of $\mu = 0$ and $\sigma = 1$.

$$p_{\text{fatal}} = F(Y|\mu = 5, \sigma = 1) = \Phi(Y - 5) \tag{32}$$

2.4.1. Thermal Harm

Equation 33 calculates the harm, as a thermal dose unit (V), from a radiant heat flux [3, 17]. This calculation uses the heat flux intensity (I, in W/m^2) and exposure time (t, in seconds). The default thermal exposure time used in the current version of HyRAM+[8] is 30 s, but users may modify this value. This default value was selected based on multiple literature sources that include the ability of a person to move away from a heat source [27, 28].

$$V = I^{(4/3)}t \tag{33}$$

The thermal probit models implemented in HyRAM+ are shown in Table 2-6 [3, 17]. The probability of a fatality due to thermal harm is evaluated using the probit value resulting from the equations in Table 2-6 with Equation 32.

Table 2-6 Thermal harm probit models where V is the thermal dose (in units of $(W/m^2)^{(4/3)}s$) [3, 17].

Model	Equation
Eisenberg [29]	$Y = -38.48 + 2.56 \times \ln(V)$
Tsao & Perry [30]	$Y = -36.38 + 2.56 \times \ln(V)$
TNO [27]	$Y = -37.23 + 2.56 \times \ln(V)$
Lees [31]	$Y = -29.02 + 1.99 \times \ln(0.5V)$

LaChance et al. [32] recommended using either the Eisenberg or the Tsao & Perry probit models for hydrogen-related assessments. The HyRAM+ default for hydrogen is the Eisenberg probit model for heat flux. This recommendation is based on the fact that hydrogen flames are less radiative than hydrocarbon flames, and so the Tsao & Perry probit model may overpredict due to the inclusion of infrared radiation. By contrast, the Tsao & Perry probit may be more relevant for hydrocarbon fuels like methane and propane; therefore, the Tsao & Perry probit is the default when methane or propane is selected as the fuel. The TNO and Lees probit accounts for clothing, which may be appropriate for some situations, though may be less conservative than the probits that do not account for clothing.

[8] The default value in HyRAM+ version 4.1 and earlier was 60 s [3, 17]

Structures can also be damaged by radiant heat flux, and it is possible that structural damage can cause physical harm (fatalities) to humans, which is the risk metric of interest within HyRAM+. However, significant structural damage would require a long radiant heat flux exposure in excess of 30 minutes [32]; the fatality risk due to thermal radiation from fires on structures and equipment is assumed to be less significant than direct thermal exposure, since people would be able to evacuate a building before thermal exposure reaches a threshold for signficant structural damage [3, 17].

2.4.2. Overpressure Harm

The probit models to predict the harm from the effects of overpressures that are implemented in HyRAM+ are shown in Table 2-7 [3]. The probability of a fatality due to overpressure is evaluated using the probit value resulting from the equations in Table 2-7 with Equation 32. In this context, the overpressure is defined as the maximum pressure above ambient.

Table 2-7 Overpressure probit models where P_s is peak overpressure (Pa) and i is the impulse of the shock wave (Pa·s) [3].

Model	Equation
Eisenberg - Lung hemorrhage [33]	$Y = -77.1 + 6.91 \ln(P_s)$
HSE - Lung hemorrhage [34, 35]	$Y = 5.13 + 1.37 \ln\left(\frac{P_s}{10^5}\right)$
TNO - Head impact [27]	$Y = 5 - 8.49 \ln\left[\frac{2430}{P_s} + \frac{4.0\times10^8}{P_s i}\right]$
TNO - Structure collapse [27]	$Y = 5 - 0.22 \ln\left[\left(\frac{40000}{P_s}\right)^{7.4} + \left(\frac{460}{i}\right)^{11.3}\right]$

LaChance et al. [32] recommended the use of the TNO probit models in hydrogen risk assessments. A person inside a structure would be more likely to be killed by the facility collapsing than from lung damage [3, 17]. However, a person located outdoors would not be at risk of a structure collapse; therefore, the HyRAM+ default is the TNO - Head Impact probit model for explosion/overpressure effects. It should be noted that some of the unconfined overpressure models in Section 3.4.5 only estimate peak overpressure, not impulse values, and so cannot be used with probit models that include an impulse term (i.e., the TNO probit models).

2.5. Risk Metrics

HyRAM+ risk calculations are done using the Potential Loss of Life (PLL) metric, which expresses the expected number of fatalities for a group of people per system-year. The PLL calculation is shown in Equation 34, where $f_{s,o}$ is the annual frequency (see Section 2.2) and $c_{s,o}$ is the consequence (see Section 2.3) of leak size s with outcome o [3, 4].

$$\text{PLL} = \sum_{s,o} f_{s,o} c_{s,o} \tag{34}$$

In order to determine the relative contribution of individual scenarios (leak size and outcome) to the total risk, the contribution to the PLL can be calculated as in Equation 35 based on the fraction of the total PLL that each individual scenario contributes.

$$\text{PLL Contribution}_{s,o} = \frac{f_{s,o} c_{s,o}}{\text{PLL}} \tag{35}$$

Another risk metric calculated by HyRAM+ is the Fatal Accident Rate (FAR), which is the expected number of fatalities for a group of people per 100 million exposed hours. The FAR is calculated using Equation 36, where N_{Pop} is the number of exposed people, h_{Year} is the number of exposed hours for the year, and dividing by 8760 converts from years to hours (exposure of 24 hours per day and 365 days per year) [3, 4, 17].

$$\text{FAR} = \text{PLL}\frac{10^8}{h_{\text{Year}}} = \text{PLL}\frac{10^8}{N_{\text{Pop}} \times 8760} \tag{36}$$

The third metric calculated in HyRAM+ is the Average Individual Risk (AIR), which is the average number of fatalities per year per exposed individual and is based on the number of hours the occupant is exposed to the hazard [4]. The AIR is calculated using Equation 37, where h_{Exposed} is the number of hours that a person spends at the facility annually (e.g., 2000 hours for a full-time worker) [3, 17].

$$\text{AIR} = \text{PLL}\frac{h_{\text{Exposed}}}{h_{\text{Year}}} = h_{\text{Exposed}} \times \text{FAR} \times 10^{-8} \tag{37}$$

2.6. Uncertainty Quantification[9]

By default, HyRAM+ calculates risk predictions deterministically, where each input is explicitly defined and set to a single value. In reality, the complexity of hydrogen systems can make having high confidence in all the needed inputs challenging and can make the resulting risk predictions potentially misleading. To address this, uncertainty quantification (UQ) methods are provided in HyRAM+ to include this uncertainty and factor it into the risk predictions.

The HyRAM+ UQ model is predicated on Monte Carlo sampling, which uses many independent pseudo-random iterations of the same simulation to quantify interacting uncertain parameters and their outcomes. HyRAM+ assumes all uncertain parameters are random variables that are probabilistically sampled from their distribution functions. Therefore, each category of uncertain inputs requires a definition of the parametric uncertainty, which includes the probability distribution type and the corresponding distribution parameters. HyRAM+ will use these parametric definitions to generate and apply the input values for the QRA for each sample. The HyRAM+ QRA model itself operates identically regardless of whether inputs are provided deterministically or probabilistically. In other words, the UQ model will run many QRA simulations, with different sampled values for the uncertain parameters applied in each QRA. The

[9]Uncertainty quantification capabilities are currently only available in the HyRAM+ Python version, not the graphic user interface (GUI) version, for HyRAM+ 6.0. This capability will be added to the GUI in a future release.

combined outputs of all the QRA simulations provides a distribution of the risk metrics of interest, which shows a more holistic picture of the risk uncertainty for a system to better inform decision making.

The allowed inputs for the UQ model are detailed in Section 2.6.1. A walkthrough of the workflow used in the UQ model is provided in Section 2.6.2. A summary of the probability distributions usable in the UQ model is provided in Section 2.6.3. An example of applying a preliminary version of the HyRAM+ UQ model to the default QRA scenario, along with a sensitivity analysis, can be found in Schroeder and Brooks [36].

2.6.1. Inputs

HyRAM+ version 6.0 allows for three categories of inputs to be uncertain. More uncertain inputs may be introduced in future releases. The parametric definitions for all categories require a basic set of distribution parameters (see Table 2-8) which are given by the user in somewhat different ways due to the specifics needed for a given category.

The three input categories that can be used in the UQ model are as follows. The report sections detailing how these variables operate at the QRA model level are given in parentheses.

- **Component Random Leak Frequency (Section 2.1.1).** Each component *and* each leak size (0.01%, 0.1%, 1%, 10%, 100%) within a single component can have a different set of distribution parameters. The quantity of each component must also be provided, as each item of a specific component type is sampled individually, with their probabilities summated when sent to the QRA model. If not provided, the component random leak frequency distributions will default to those given in Table 2-2.
- **Dispenser Release Probabilities (Section 2.1.4).** Each failure mode for all fueling components and accidents can be given its own distribution, with the overall frequency of a dispenser release utilized by the QRA model. If not provided, the dispenser release and accident probabilities will default to those given in Table 2-3 and Table 2-4.
- **Occupant Location (Section 2.3.1).** Each coordinate direction can be given its own distribution. Different groups can also be defined, each with its own distribution parameters. The number of occupants in each group must also be provided.

2.6.2. Workflow

The HyRAM+ UQ model follows the following procedure:

1. **Input parsing:** HyRAM+ takes the distribution parameters and quantities for each uncertain input category and arranges them into individual uncertain items to sample. For example, if a system has three filters, HyRAM+ will split each of the filters and each leak size per filter into its own item to sample the random leak frequencies individually.

2. **Sampling:** HyRAM+ samples each uncertain item from their defined probability distributions. The user sets the number of samples as an input to the UQ model. The user also sets whether the sampling is performed using simple random sampling or Latin hypercube sampling, which is a sampling method designed to ensure more efficient coverage of the full input space than simple random sampling [37].
3. **Formulate QRA inputs:** HyRAM+ recombines the individually sampled items into a format that can be used to the HyRAM+ QRA model. For example, HyRAM+ sums the individual component leak frequencies for each leak size to provide a total sampled random leak frequency for each leak size of a given component type.
4. **Model samples in QRA:** The UQ model sends sets of samples to the HyRAM+ QRA model, and each set of samples functions as inputs to a standard QRA simulation. If the computer has multiple CPU cores available, the QRA simulations will run in parallel to reduce execution time.
5. **Compile QRA results:** Once all QRA simulations are complete, HyRAM+ collects the QRA outputs (see Section 2.5) for all simulations and returns them to the user.

2.6.3. Distributions

The HyRAM+ UQ model supports several types of probability distributions, which are outlined below in Table 2-8. The UQ model is built from the SciPy statistics Python package (`scipy.stats`) [38]; more specifics on the listed probability distributions can be found in the SciPy user documentation[10]. Note that some variables can be specified as deterministic even if other variables in the same definition set are given probabilistically. Additionally, the model supports different probability distribution parameters for each specific fault tree item. For example, the user could specify a lognormal distribution for dispenser releases for overpressure accidents, but a beta distribution for driveoff accidents.

Table 2-8 Probability distributions available in the HyRAM+ uncertainty quantification model.

Distribution	Input Parameters
Deterministic	Value
Normal	μ, σ
Lognormal	μ, σ
Beta	α, β
Truncated Normal	μ, σ, Lower & Upper Bounds
Truncated Lognormal	μ, σ, Lower & Upper Bounds
Uniform	Lower & Upper Bounds

[10] see `https://docs.scipy.org/doc/scipy/reference/stats.html`

3. PHYSICS MODELS

HyRAM+ includes physical models relevant to the behavior, hazards, and consequences of releases of different fuels [3]. Some of these models are used in QRA analyses to determine the consequences of a release, as described in Section 2.3, but can also be exercised as independent analyses. Jet flames, concentration profiles for unignited jets/plumes, overpressure from the delayed ignition of a plume, and indoor accumulation with delayed ignition causing overpressure can all be analyzed. Several basic property calculations (e.g., the thermodynamic equation of state) are necessary to numerically simulate the release scenarios.

3.1. Properties of the Fluids

The formulations in this section describe the thermodynamic properties of unignited and ignited hydrogen, methane, propane, and blends, which are needed to calculate different aspects of dispersion and combustion [12]. They are described here in detail, and then referred to in subsequent sections [3].

3.1.1. Equation of State

Description: HyRAM+ utilizes the CoolProp library [39], called through its Python interface to perform several thermodynamic calculations [14]. The property calculations are based on a Helmholtz energy function, and account for the real gas behavior at high pressures and at liquid (which can be cryogenic) temperatures, for liquids, gases, and two-phase mixtures. CoolProp [39] can be used to calculate the properties of hydrogen, methane, propane, air, or other fluids, including blends. For hydrogen, the relationships and energy functions are detailed in Leachman et al. [40], for methane, in Setzmann and Wagner [41], and for propane, in Lemmon et al. [42]. CoolProp handles blends following the work of Kunz et al. [43, 44] and Lemmon et al. [45–47]. The mixing parameters for the fluids available in the front-end of HyRAM+ are from Kunz et al. [43, 44]. These thermodynamic calculations are used to calculate leak rates and are used in mass, momentum, and energy balances in regions close to the leak point. As an example, for hydrogen, the relationships between pressure[11], temperature, density, enthalpy, and entropy are plotted in Figure 3-1. In some regions of the models, the ideal gas equation of state is used, as described in other sections.

[11] HyRAM+ calculation inputs use absolute pressure, not gauge pressure

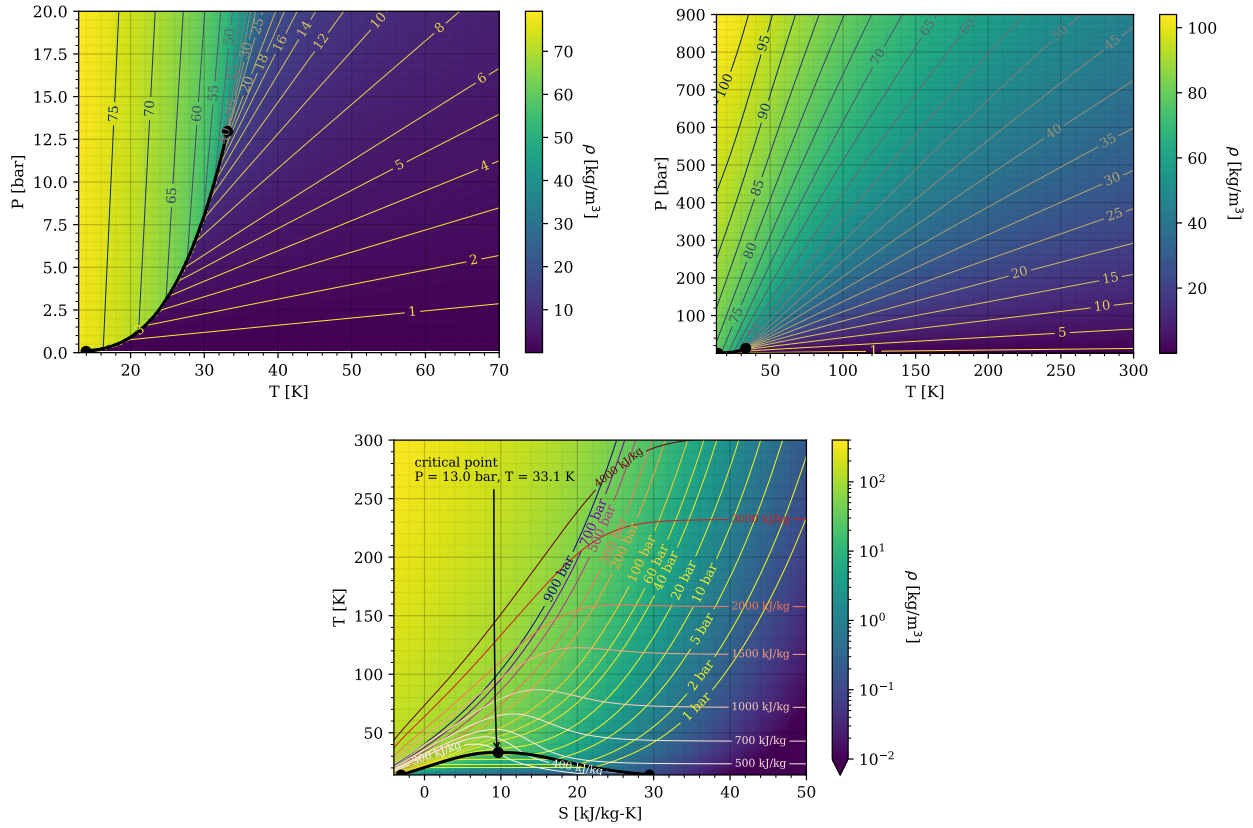

Figure 3-1 Graphical representations of state points, calculated using CoolProp [39] which uses the Leachman et al. [40] equation of state for hydrogen. Top plots show shading and iso-contours of density as a function of temperature and pressure. Bottom plot shows shading of density as a function of entropy and temperature, with iso-contours of pressure and enthalpy. The thick black line shows the liquid/two-phase/vapor boundary, and the black dots mark the triple point and critical points.

Applicability: The fundamental equation of state described by Leachman et al. [40] is valid for hydrogen at pressures up to 2000 MPa and between 14 K and 1000 K [14]. The equation of state for methane described by Setzmann and Wagner [41] is valid from 90 K to 620 K at pressures up to 1000 MPa. The relationships described by Lemmon et al. [42] are valid for propane from 85.5 K to 650 K and for pressures up to 1000 MPa. The most accurate range of validity for mixtures/blends is for temperatures from 90 K to 450 K and pressures up to 35 MPa, although limited data extends validity from 60 K to 700 K and up to 70 MPa [44]. Note that there is no check that the equation of state is being used within the stated validation limits and HyRAM+ can calculate outputs for temperatures and pressures outside the range of validity using the same equation of state [12].

3.1.2. Combustion

Description: HyRAM+ flame calculations are based on the work of Ekoto et al. [48] and rely on several underlying properties of burned fuel, namely the stoichiometric mixture fraction, f_s,

the heat of combustion, ΔH_c, along with the temperature, molecular weight, and density of combustion products for a given mixture fraction [14].

Assumptions: Combustion is only assumed to occur in expanded fuel at atmospheric pressure [14]. Because combustion occurs at ambient pressure, the ideal gas equation is used to calculate the density of the product mixture (ρ) based on the molecular weight of the mixture ($\mathrm{MW}_{\mathrm{mixture}}$), the temperature ($T$), and the gas constant (R):

$$\rho = \frac{P(\mathrm{MW}_{\mathrm{mixture}})}{RT}. \tag{38}$$

These combustion calculations assume that there are no losses, that the mixture is thermally perfect with the local enthalpy, and the pressure of the products is the same as the pressure of the reactants [14].

Relationships: It is assumed that there are fuels and inerts reacting with pure air, and complete combustion drives the products to water and carbon dioxide [10]. For each mole of carbon as a reactant, 1 mole O_2 is needed as a reactant and 1 mole of CO_2 will be produced. For each mole of hydrogen as a reactant, 1/4 mole of O_2 is needed as a reactant to produce 1/2 mole of H_2O. For each mole of oxygen in the reactants (for example, in CO_2), 1/2 mole less of O_2 is needed as a reactant. Therefore, the moles of oxygen needed as a reactant is

$$\nu_{O_2} = n_C + \frac{n_H}{4} - \frac{n_O}{2} \tag{39}$$

where n is the moles of each species (subscripts C - carbon, H - hydrogen, O - oxygen) in the fuel. For example, hydrogen (H_2) has 2 moles of hydrogen and requires $2/4 = 1/2$ mole of O_2, methane (CH_4) has 4 moles of hydrogen and 1 mole of carbon and requires $1 + 4/4 = 2$ moles of O_2, and propane (C_3H_8) has 3 moles of carbon and 8 moles of hydrogen and therefore requires $3 + 8/4 = 5$ moles of O_2 for complete combustion. For blends, the moles of carbon, hydrogen, and oxygen are often non-integers.

During combustion, 242 kJ is released for every mole of gaseous water produced, and 394 kJ is released for every mole of carbon dioxide produced [49]. Therefore, when hydrogen is the fuel, the heat of combustion is 242 $\mathrm{kJ/mol}_{H_2}$ or 120 $\mathrm{MJ/kg}_{H_2}$ (using the lower heating value) [50, 51]. For methane and propane, the heats of combustion are 50 MJ/kg and 46.4 MJ/kg, respectively. The values can be calculated for other fuels in a similar manner. The heat of combustion from a blend is weighted based on the mass fraction of each reactant in the fuel.

From the moles of oxygen required for complete combustion (Eq. 39), the stoichiometric mixture fraction (f_s), which is the same as the mass fraction of fuel, can be calculated as:

$$f_s = \frac{\mathrm{MW}_{\mathrm{fuel}}}{\mathrm{MW}_{\mathrm{fuel}} + \nu_{O2}(\mathrm{MW}_{O_2} + 3.76\mathrm{MW}_{N_2})}. \tag{40}$$

The stoichiometric mixture fractions for hydrogen, methane, and propane are 0.02852, 0.05519, and 0.06034 respectively [12]. If incomplete combustion occurs (a mixture fraction other than stoichiometric), there will be excess air or fuel as a reactant, with the stoichiometry given by

$$\begin{aligned}(\text{fuel}) + \eta\nu_{O_2}\,(O_2 + 3.76N_2) \rightarrow\ & \max(0, 1-\eta)(\text{fuel}) \\ & + \frac{n_H}{2}\cdot\min(1,\eta)H_2O + n_C\cdot\min(1,\eta)CO_2 \\ & + \max\left(0, (\eta-1)\nu_{O_2}\right)O_2 + 3.76\eta\nu_{O_2}N_2, \end{aligned} \tag{41}$$

where η, which specifies the moles of air, can vary from 0 to ∞ [12]. In this case, the mixture fraction is equal to

$$f = Y_{\text{fuel}} + Y_{H_2O}\frac{\text{MW}_{\text{fuel}}}{\text{MW}_{H_2O}} + Y_{CO_2}\frac{\text{MW}_{\text{fuel}}}{\text{MW}_{CO2}}, \tag{42}$$

where Y is the mass fraction of products [12]. HyRAM+ uses CoolProp [39] to calculate the mass fraction weighted enthalpy (h) of the fuel along with the enthalpy of H_2O, CO_2, O_2, and N_2 as a function of temperature and then solves for the temperature of products assuming an isenthalpic reaction [14], i.e.,

$$\begin{aligned}\sum_{i=\text{fuel},O_2,N_2} Y_{i,\text{reac}}h_{i,\text{reac}}(T_{\text{reac}}, P_{\text{reac}}) = & \sum_{i=\text{fuel},O_2,N_2,CO_2,H_2O} Y_{i,\text{prod}}h_{i,\text{prod}}(T_{\text{prod}}, P_{\text{prod}}) \\ & + Y_{H_2O,\text{prod}}\frac{\text{MW}_{\text{fuel}}}{(n_C+1)\text{MW}_{H_2O}}\Delta H_c. \end{aligned} \tag{43}$$

The calculation of the adiabatic flame temperature (T_{ad}) and density of the products of 298 K, 101,325 Pa pure fuels are shown in Figure 3-2 [12].

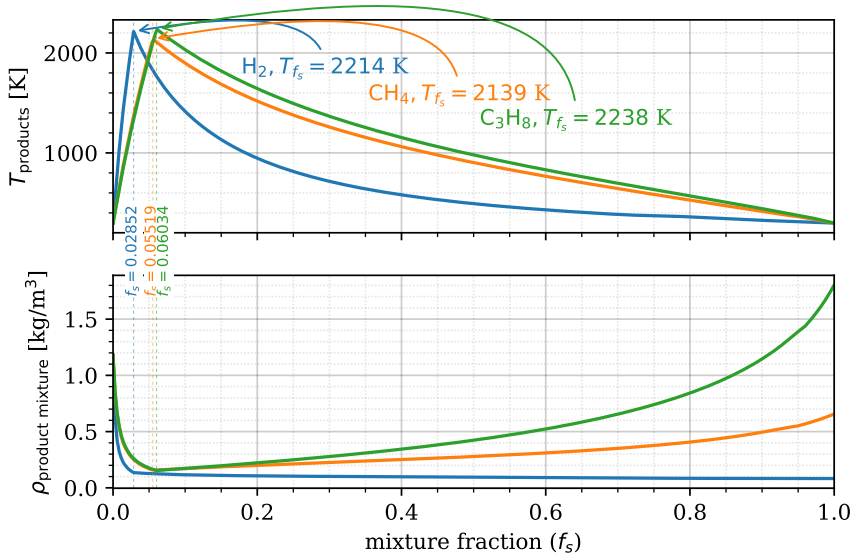

Figure 3-2 Temperature and density of products for the combustion of 298 K, 101,325 Pa fuels as a function of mixture fraction [12].

Applicability: These combustion calculations are applicable in atmospheric pressure regions where heat losses are negligible [14].

3.2. Developing Flow

Several engineering models are used in HyRAM+ to develop boundary conditions for the integral models of jets/plumes and diffusion flames [11]. These engineering models describe the flow through an orifice, how the fluid expands to atmospheric pressure (if necessary), how the fluid warms to a level that the equation of state is valid (if necessary), and finally how the flow develops into the Gaussian profiles that serve as the boundary conditions to the models described in Sections 3.3.1 and 3.4.2.

3.2.1. Orifice Flow

HyRAM+ assumes that fluids flow isentropically through an orifice [14]. CoolProp [39] is used to calculate the entropy (s_0) and enthalpy (h_0) of the fluid upstream of an orifice, using the specified pressure and temperature (or phase if a saturated vapor or saturated liquid is specified). CoolProp [39] is then used to calculate the enthalpy (h) and density (ρ) of a fluid at a given pressure with the same entropy as the upstream fluid (s_0). An isenthalpic expansion requires

$$\frac{v^2}{2} + h = h_0 \tag{44}$$

which can be solved for the velocity, v, and the mass flux can be calculated as

$$\dot{m}'' = \rho v. \tag{45}$$

A maximum mass flux is sought between the ambient and upstream pressures [52–54] using a bounded solver [11]. If the maximum mass flux occurs at atmospheric pressure, the flow is unchoked, while if the maximum mass flux is at a pressure above atmospheric, the flow is choked. In the case of choked flow, the velocity through the orifice will be the speed of sound for the given throat conditions. The choked flow speed of sound for gases is the same as that calculated by CoolProp [39], but this algorithm also works for two-phase and liquid flows through the throat, for which the speed of sound is ill-defined.

Orifices in HyRAM+ are assumed to be circular, characterized by their diameter, d, and a coefficient of discharge, C_d [3]. When the velocity and density of the fluid at the orifice is known, the mass flow rate is calculated as:

$$\dot{m} = \frac{\pi}{4} d^2 \dot{m}'' C_d = \frac{\pi}{4} d^2 \rho v C_d. \tag{46}$$

3.2.2. Notional Nozzles

Notional nozzles are used to calculate the effective diameter, velocity, and thermodynamic state after the complex shock structure of an under-expanded jet [3]. In HyRAM+, a notional nozzle model is used if the pressure at the orifice is above atmospheric pressure [14]. They are not necessarily a physical description of the phenomena, but a jet with the diameter, velocity and state (temperature and atmospheric pressure) of the notional nozzle would lead to the same dispersion

characteristics as the underexpanded jet. There are five different notional nozzle models in HyRAM+, with each model conserving mass between flow through the real orifice and flow through the notional nozzle. This means that

$$\rho_{\text{eff}} v_{\text{eff}} A_{\text{eff}} = \rho_{\text{throat}} v_{\text{throat}} A_{\text{throat}} C_D \tag{47}$$

where ρ is the density, v is the velocity, A is the cross-sectional area, C_D is the discharge coefficient, the subscript "throat" denotes the choke point (at the orifice, see Section 3.2.1), and the subscript "eff" denotes effective (after the shock structure and the pressure has returned to atmospheric).

The default notional nozzle model in HyRAM+ is based on the work of Yüceil and Ötügen [55]. In this case, mass (Equation 47), momentum, and energy are conserved [14]. Conservation of momentum is written as

$$\rho_{\text{eff}} v_{\text{eff}}^2 A_{\text{eff}} = \rho_{\text{throat}} v_{\text{throat}}^2 A_{\text{throat}} C_D + A_{\text{throat}} (P_{\text{throat}} - P_{\text{ambient}}) \tag{48}$$

where P is the pressure. Simultaneous solution of Equations 47 and 48 yields a solution for the velocity at the notional nozzle

$$v_{\text{eff}} = v_{\text{throat}} C_D + \frac{P_{\text{throat}} - P_{\text{ambient}}}{\rho_{\text{throat}} v_{\text{throat}} C_D} \tag{49}$$

and the effective area of the notional nozzle

$$A_{\text{eff}} = \frac{\rho_{\text{throat}} v_{\text{throat}}^2 A_{\text{throat}} C_D^2}{\rho_{\text{eff}} \left(P_{\text{throat}} - P_{\text{ambient}} + \rho_{\text{throat}} V_{\text{throat}}^2 C_D^2 \right)} \tag{50}$$

The effective area calculation in Equation 50 requires the effective density, which can be calculated using the conservation of energy (assuming isentropic expansion), where

$$\frac{v_{\text{eff}}^2}{2} + h(\rho_{\text{eff}}, P_{\text{ambient}}) = \frac{v_{\text{throat}}^2}{2} + h_{\text{throat}}. \tag{51}$$

CoolProp [39] is used to calculate the enthalpy and Equation 51 is iteratively solved to determine the effective density.

Alternative to using Equation 51, the second notional nozzle model follows the work of Birch et al. (1987) [56]. In this work, the effective density is calculated by assuming that the temperature of the notional nozzle is the same as the temperature of the stagnant gas, or

$$\rho_{\text{eff}} = \rho(T_0, P_{\text{ambient}}) \tag{52}$$

where T_0 is the temperature of the stagnant gas (storage temperature) and CoolProp [39] is used to calculate the density.

Three other notional nozzle models do not conserve momentum (Equation 48), but rather assume that the notional nozzle velocity is at the speed of sound, as follows. The third notional nozzle model follows the work of Birch et al. (1984) [57]. For this model, it is assumed that the

temperature at the notional nozzle is the same as temperature of the stagnant gas, the density (see Equation 52) and velocity at the notional nozzle can be calculated

$$v_{\text{eff}} = a(T_0, P_{\text{ambient}}) \tag{53}$$

where a is the speed of sound, calculated using CoolProp [39]. The conservation of mass, Equation 47, along with Equations 52 and 53, can be used to specify the notional nozzle conditions.

Alternatively, Ewan and Moody [58] use the assumption that the temperature at the notional nozzle is the same as the temperature at the throat, or

$$\rho_{\text{eff}} = \rho(T_{\text{throat}}, P_{\text{ambient}}) \tag{54}$$

$$v_{\text{eff}} = a(T_{\text{throat}}, P_{\text{ambient}}). \tag{55}$$

Finally, Molkov et al. [59] specifies that mass and energy are conserved between the orifice and the notional nozzle and that the notional nozzle is at the speed of sound, i.e., Equation 47 along with the simultaneous solution of the equations,

$$\frac{v_{\text{eff}}^2}{2} + h(\rho_{\text{eff}}, P_{\text{ambient}}) = \frac{v_{\text{throat}}^2}{2} + h_{\text{throat}} \tag{56}$$

$$v_{\text{eff}} = a(\rho_{\text{eff}}, P_{\text{ambient}}) \tag{57}$$

where h and a are calculated using CoolProp [39].

To summarize, the 5 different notional nozzles available in HyRAM+ solve the equations [14]:

- (default) Yüceil and Ötügen [55]: Equations 49, 50, and 51
- Birch et al. (1987) [56]: Equations 49, 50, and 52
- Birch et al. (1984) [57]: Equations 47, 52, and 53
- Ewan and Moody [58]: Equations 47, 54, and 55
- Molkov et al. [59]: Equations 47, 56, and 57

3.2.3. Initial Entrainment and Heating

The models in HyRAM+ are valid for hydrogen, methane, propane, and blends, including saturated vapor and saturated liquid releases [12]. Specifically for cryogenic hydrogen, there are challenges calculating properties in regions of the flow where oxygen and nitrogen from the entrained air would condense due to the extremely low temperatures, as noted by Houf and Winters [60]. To account for this, conservation of mass, energy and momentum can be applied until the temperature of the mixture (still assumed to be a plug-flow) is above a specified temperature (T_{min}). However, it should be noted that the default minimum temperature is 0 K, so initial entrainment and heating is currently unused in the GUI implementation and can only be used in the Python implementation. If the temperature of the notional nozzle (or at the orifice, if

the flow is unchoked) is below T_{min}, the state after initial entrainment and heating is specified as the fuel at T_{min}, and simultaneous solution to the momentum and energy balances yields the mass fraction of fuel (Y) when the mixture has warmed to T_{min}, i.e.,

$$\dot{m}_{\text{out}} = \dot{m}_{\text{in}} + \frac{1-Y}{Y}\dot{m}_{\text{in}} \tag{58}$$

$$v_{\text{out}} = v_{\text{in}}\frac{\dot{m}_{\text{in}}}{\dot{m}_{\text{out}}} \tag{59}$$

$$h_{\text{out}} = (1-Y)h_{\text{air}}(T_{min}, P_{\text{ambient}}) + Y h_{\text{H}_2}(T_{min}, P_{\text{ambient}}) + \frac{v_{\text{out}}^2}{2} \tag{60}$$

$$\dot{m}_{\text{out}}h_{\text{out}} = \dot{m}_{in}h_{\text{in}} + (\dot{m}_{\text{out}} - \dot{m}_{\text{in}})h_{\text{air}}(T_{\text{ambient}}, P_{\text{ambient}}). \tag{61}$$

Once the mass fraction (Y) is known, conservation of mass is used to yield the diameter of the plug flow at the end of the zone of initial entrainment and heating,

$$\rho_{\text{out}} = \frac{1}{\frac{1-Y}{\rho_{\text{air}}(T_{min},P_{\text{ambient}})} + \frac{Y}{\rho_{\text{H}_2}(T_{min},P_{\text{ambient}})}} \tag{62}$$

$$d_{\text{out}} = \sqrt{\frac{\pi\dot{m}_{\text{out}}}{4\rho_{\text{out}}v_{\text{out}}}} \tag{63}$$

and the momentum driven entrainment rate (see Equation 87) is used to calculate the length of this zone,

$$S_{\text{out}} = \frac{(1-Y)(\dot{m}_{\text{out}} - \dot{m}_{\text{in}})}{\rho_{\text{ambient}}(T_{\text{ambient}}, P_{\text{ambient}})E_{mom}}. \tag{64}$$

3.2.4. Establishment of a Gaussian Profile

The flows described in Sections 3.2.1, 3.2.2, and 3.2.3 are all assumed to be plug flows, where the properties (e.g., velocity, density) are constant across the entire cross-section of the flow [14]. However, jets, plumes, or flames from a pure source are well-known to have Gaussian profiles of their properties (e.g., velocity, density, mixture fraction) in the downstream regions [48, 61]. The final model for developing flow describes the transition from plug flow to the Gaussian profile that is used as an input to a one-dimensional system of ordinary differential equations that describes unignited dispersion or a diffusion flame (see Sections 3.3.1 and 3.4.2). Following the work of Winters [62], the centerline velocity of the Gaussian flow is assumed to be equivalent to the plug flow velocity, the jet is characterized by a half-width, B, where the velocity drops to half of the center-line value, and a spreading ratio, λ, the ratio of density spreading relative to velocity. The center-line (denoted with a cl subscript) mass-fraction is related to λ via the relationship,

$$\frac{\lambda^2+1}{2\lambda^2} = \frac{Y_{cl} - Y_{\text{ambient}}}{Y_{\text{plug}} - Y_{\text{ambient}}}. \tag{65}$$

Then the center-line molecular weight can be calculated,

$$\text{MW}_{cl} = \frac{1}{Y_{cl}/\text{MW}_{\text{fuel}} + (1-Y_{cl})/\text{MW}_{\text{air}}}. \tag{66}$$

The heat capacity of the fluid and ambient air are determined from CoolProp [39] and used to calculate the individual and mixture enthalpies as $h = c_p \cdot T$, where

$$c_{p,\text{plug}} = c_{p,\text{C}_\text{n}\text{H}_{2\text{n}+2}} Y_{\text{plug}} + c_{p,\text{air}}(1 - Y_{\text{plug}}), \tag{67}$$

$$c_{p,cl} = c_{p,\text{plug}} Y_{cl} + c_{p,\text{air}}(1 - Y_{cl}), \tag{68}$$

$$\frac{\lambda^2 + 1}{2\lambda^2} = \frac{h_{cl} - h_{\text{ambient}}}{h_{\text{plug}} - h_{\text{ambient}}}. \tag{69}$$

From these equations, the center-line temperature can be calculated, and the center-line density is calculated using the ideal gas equation of state, where

$$\rho_{cl} = \frac{\text{MW}_{cl} P}{R T_{cl}}. \tag{70}$$

The length of the developing flow region is a function of the densimetric Froude number[12], as described by Winters [62]. The densimetric Froude number and plug flow diameter are based either on the flow from the orifice (as described in Section 3.2.1), or on the expanded orifice (described in Section 3.2.2) after initial entrainment and heating (described in Section 3.2.3), if those either or both of those engineering models are applied. The starting point of the streamline coordinate, S_0 for the Gas Jet/Plume model (Section 3.3.1) or the Jet Flame model (Section 3.4.2) is given by

$$\frac{S_0 - S_{\text{out}}}{d_{out}} = \begin{cases} 6.2 & \text{Fr}_{\text{den}}{}^2 \geq 40 \\ 3.9 + 0.057\text{Fr}_{\text{den}}{}^2 & 5 \leq \text{Fr}_{\text{den}}{}^2 < 40 \\ 2.075 + 0.425\text{Fr}_{\text{den}}{}^2 & 1 \leq \text{Fr}_{\text{den}}{}^2 < 5 \\ 0 & 0 \leq \text{F}_{\text{den}}{}^2 < 1 \end{cases}, \tag{71}$$

where

$$\text{Fr}_{\text{den}} = \frac{v_{\text{out}}}{\sqrt{g d_{\text{out}} |\rho_\infty - \rho_{\text{out}}| / \rho_{\text{out}}}}. \tag{72}$$

3.3. Unignited Releases

3.3.1. Gas Jet/Plume

For a jet or plume, HyRAM+ follows the one-dimensional model described by Houf and Winters [60]. While the model only considers one dimension, this dimension is along the streamline, and the jet/plume can curve due to buoyancy effects (or wind, although this aspect is not currently included) [3]. The reduction in dimension comes from the assumption that the mean

[12] In HyRAM+ versions 5.1 and previous, this length was fixed at $S/d = 6.2$, which was valid for high densimetric Froude numbers

profiles of the velocity (v), density (ρ), and product of density and mass fraction (Y) of fuel are Gaussian, as

$$v = v_{cl} \exp\left(-\frac{r^2}{B^2}\right) \tag{73}$$

$$\rho = (\rho_{cl} - \rho_{amb}) \exp\left(-\frac{r^2}{\lambda^2 B^2}\right) + \rho_{amb} \tag{74}$$

$$\rho Y = \rho_{cl} Y_{cl} \exp\left(-\frac{r^2}{\lambda^2 B^2}\right) \tag{75}$$

where B is a characteristic half-width, λ is the ratio of density spreading relative to velocity, the subscript cl denotes the centerline, the subscript amb denotes ambient, and r is perpendicular to the stream-wise direction. Gravity acts in the negative y-direction, and the plume angle, θ is relative to the x-axis (horizontal), as shown in Figure 3-3.

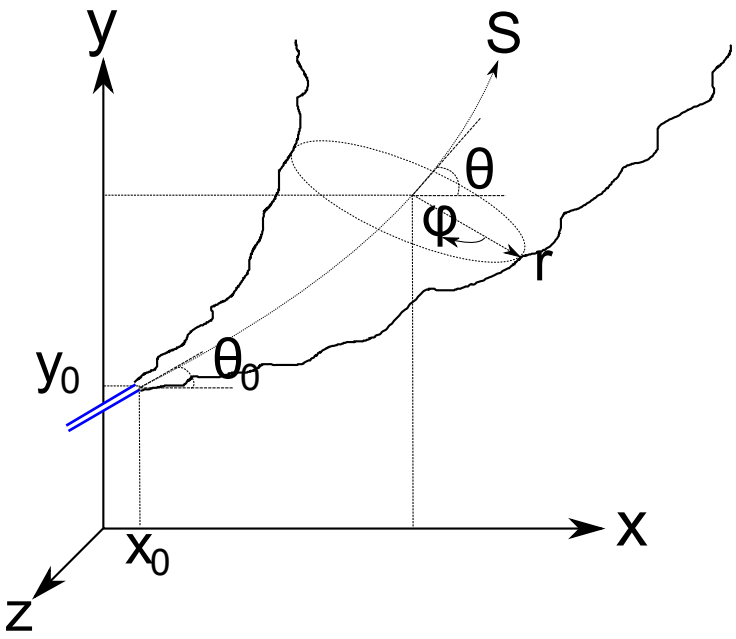

Figure 3-3 Sketch of plume model coordinates [3]. Gravity acts in the negative y-direction.

The derivatives of the spatial dimensions are therefore

$$\frac{dx}{dS} = \cos\theta, \tag{76}$$

$$\frac{dy}{dS} = \sin\theta. \tag{77}$$

The conservation equations can be written as follows:

continuity:

$$\frac{d}{dS}\int_0^\infty (\rho v) 2\pi r dr = \rho_{amb} E, \tag{78}$$

x-momentum:

$$\frac{d}{dS}\int_0^\infty \left(\rho v^2 \cos\theta\right) 2\pi r dr = 0, \tag{79}$$

y-momentum:

$$\frac{d}{dS}\int_0^\infty \left(\rho v^2 \sin\theta\right) r dr = \int_0^\infty (\rho_{amb} - \rho) g r dr, \tag{80}$$

species continuity:

$$\frac{d}{dS}\int_0^\infty (\rho v Y)\, 2\pi r dr = 0, \tag{81}$$

energy:

$$\frac{d}{dS}\int_0^\infty \rho v \left(h + \frac{v^2}{2} - h_{amb}\right) 2\pi r dr = 0. \tag{82}$$

Similar to Houf and Winters [60], HyRAM+ assumes that $h = c_p T$ and the ideal gas equation of state is used for these ambient pressure mixtures [14]. The mixture molecular weight, heat capacity, and product of density and enthalpy all vary with respect to the radial coordinate (due to the fact that Y and ρ vary radially, see Equation 75) according to the following expressions:

$$\mathrm{MW} = \frac{\mathrm{MW}_{amb}\mathrm{MW}_{\mathrm{fuel}}}{Y(\mathrm{MW}_{amb} - \mathrm{MW}_{\mathrm{fuel}}) + \mathrm{MW}_{\mathrm{fuel}}}, \tag{83}$$

$$c_p = Y(c_{p,\mathrm{fuel}} - c_{p,amb}) + c_{p,amb}, \tag{84}$$

$$\rho h = \frac{P}{R} c_p \mathrm{MW}. \tag{85}$$

The Gaussian profiles in Equations 73-75 are plugged into the governing equations, and with the exception of the energy equation can be integrated analytically [14]. For the energy equation, Equation 82, the numeric integration to infinity is estimated by evaluation to $5B$. This results in a system of 7 first order differential equations where the independent variable is S and the dependent variables are v_{cl}, B, ρ_{cl}, Y_{cl}, θ, x, and y. This system of equations is integrated from the starting point to the distance desired using an explicit Runge-Kutta method of order (4)5.

The entrainment model follows Houf and Schefer [61], where there is a combination of momentum and buoyancy driven entrainment [3],

$$E = E_{mom} + E_{buoy}, \tag{86}$$

where

$$E_{mom} = 0.282 \left(\frac{\pi d_{\mathrm{exp}}^2}{4} \frac{\rho_{\mathrm{exp}} v_{\mathrm{exp}}^2}{\rho_\infty}\right)^{1/2}, \tag{87}$$

where the "exp" subscript denotes after the notional nozzle and zone of initial entrainment and heating (if used; see Sections 3.2.2 and 3.2.3), and

$$E_{buoy} = \frac{a}{\mathrm{Fr}_l}(2\pi v_{cl} B)\sin\theta, \tag{88}$$

where the local Froude number,

$$\mathrm{Fr}_l = \frac{v_{cl}^2}{gD(\rho_\infty - \rho_{cl})/\rho_{\mathrm{exit}}}. \tag{89}$$

In these equations, a is empirically determined:

$$\begin{cases} a = 17.313 - 0.116665\mathrm{Fr}_{\mathrm{den}} + 2.0771\times10^{-4}\mathrm{Fr}_{\mathrm{den}}{}^2, & \mathrm{Fr}_{\mathrm{den}} < 268 \\ a = 0.97, & \mathrm{Fr}_{\mathrm{den}} \geq 268, \end{cases} \tag{90}$$

with the densimetric Froude number given in Eq. 72.

As the jet/plume becomes buoyancy-dominated (as opposed to momentum-dominated), the non-dimensional number

$$\alpha = \frac{E}{2\pi B v_{cl}} \tag{91}$$

will increase. When α reaches the limiting value of $\alpha = 0.082$, α is held constant and the entrainment value becomes:

$$E = 2\pi\alpha B v_{cl} = 0.164\pi B v_{cl}. \tag{92}$$

Mole fractions are used in many analyses, which are calculated after solving the system of equations using the mass fraction and molecular weight as

$$X = Y\frac{\mathrm{MW}}{\mathrm{MW}_{\mathrm{fuel}}} \tag{93}$$

3.3.2. Tank Mass

The mass of fuel in a storage container (m) is calculated using the density of the fuel (ρ) and fixed volume of the container (V) using Equation 94 [15]. The density of the fuel (ρ) is calculated using the specified temperature and pressure using the CoolProp library [39] as described in Section 3.1.1.

$$m = \rho V \tag{94}$$

3.3.3. Tank Emptying

In the case of a storage tank with a given volume, the transient process of the tank emptying (blowdown) can also be calculated by HyRAM+ [15]. In this case, energy and mass are conserved [14], following the work of Hosseini et al. [63]. The mass flow rate $\dot{m}$ is calculated as described in Section 3.2.1, whether the flow is choked or not. Energy is conserved in the tank volume, where

$$\frac{du}{dt} = \frac{\dot{m}(h-u)+q}{m}, \tag{95}$$

where u and h are the specific energy and specific enthalpy (J/kg), respectively, of the fuel in the tank (calculated using CoolProp [39]), m is the mass of fuel in the tank (kg, see Section 3.3.2), and q is the heat flow into the tank (J/s, $q = 0$ if adiabatic). This equation and the equations describing the mass flow rate (which are functions of the pressure and temperature inside the tank) are integrated until the mass or pressure in the tank reaches the desired stopping point (e.g., the tank pressure reaches ambient).

3.3.4. Accumulation in Confined Areas/Enclosures

When a release occurs in an enclosure, a stratified mixture of fuel and air can accumulate [3]. For hydrogen or methane, the accumulated mixture will be near the ceiling due to buoyancy [12].

The release inside an enclosure can be assumed to come from some tank with a fixed volume [14]. Therefore, the flow from the tank follows Section 3.3.3. At each point in time for the blowdown, the jet/plume is modeled as described in Section 3.3.1. The release can also be assumed to come from a steady-state source.

When these releases occur indoors, the plumes could impinge on a wall [3]. Currently, should this impingement happen, the trajectory of the jet/plume is modified such that the fuel will travel vertically upwards along the wall, rather than in the horizontal direction, with the same features (e.g., half-width, centerline velocity). Note that this deflection upwards will occur regardless of the fuel and is a poor assumption for heavier fuels such as propane.

Accumulation occurs following the model of Lowesmith et al. [64], where a layer forms along the ceiling [3]. Conservation of mass requires that

$$\frac{dV_l}{dt} = Q_{\text{in}} - Q_{\text{out}}, \tag{96}$$

where V_l is the volume of gas in the layer, and Q is the volumetric flow rate, with subscript "in" referring to the flow rate of fuel and air entrained into the jet at the height of the layer, and "out" referring to flow out the ventilation. Species conservation requires that

$$\frac{d(\chi V_l)}{dt} = Q_{\text{leak}} - \chi Q_{\text{out}}, \tag{97}$$

where χ is the mole or volume fraction of fuel in the layer and Q_{leak} is the leak rate of the fuel. Expanding the derivative and substituting Equation 96 yields

$$V_l \frac{d\chi}{dt} = Q_{\text{leak}} - \chi Q_{\text{in}}. \tag{98}$$

Q_{in} is solved for by modeling a jet/plume within the enclosure to calculate the jet half-width (B) and centerline velocity (v_{cl}), as described in Section 3.3.1 at the height of the bottom of the layer. The volumetric flow rate (Q_{in}) is calculated as:

$$Q_{\text{in}} = \pi B^2 v_{cl}. \tag{99}$$

Flows out of the enclosure are driven by buoyancy, and potentially wind or a fan. Buoyancy driven flow is calculated as

$$Q_b = C_d A_v \sqrt{g' H_l}, \tag{100}$$

where C_d is a coefficient of discharge, A_v is the area of the upper (outlet) vent, H_l is the height of the layer (between the bottom of the layer and the center-point of the outlet vent), and g' is reduced gravity:

$$g' = g \frac{\rho_{\text{air}} - \rho_l}{\rho_{\text{air}}}, \tag{101}$$

where g is the gravitational constant, ρ_l is the density of the layer, and ρ_{air} is the density of air (at the temperature and pressure of the enclosure). The density in the layer (ρ_l) is calculated from the density of air (ρ_{air}) and the density of the fuel ($\rho_{\text{C}_n\text{H}_{2n+2}}$), both at the temperature and pressure of the enclosure, as:

$$\rho_l = \chi \rho_{\text{C}_n\text{H}_{2n+2}} + (1 - \chi)\rho_{\text{air}}. \tag{102}$$

Wind (or mechanical ventilation) is assumed to drive the flow at a rate of:

$$Q_w = \frac{C_d A_v U_w}{\sqrt{2}} = \frac{C_d Q_{\text{vent}}}{\sqrt{2}}, \tag{103}$$

where C_d is a coefficient of discharge, A_v is the area of the lower (inlet) vent, U_w is the velocity of the wind (or mechanical ventilation) through the lower (inlet) vent, and Q_{vent} is the volumetric flow rate through the lower (inlet) vent ($Q_{\text{vent}} = A_v U_w$). Note that Q_{vent} is a user input.

The total flow out of the enclosure, accounting for buoyancy driven flow and flow from the vent, is calculated as

$$Q_{\text{out}} = Q_{\text{leak}} + \sqrt{Q_b^2 + Q_w^2}. \tag{104}$$

3.4. Ignited Releases

3.4.1. Flame Correlations

As noted by Houf and Schefer [65], a non-dimensional flame length, defined as

$$L^* = \frac{L_{\text{vis}} f_s}{d_j \sqrt{\rho_j / \rho_{amb}}} \tag{105}$$

collapses onto a single curve for a range of fuels (hydrogen, methane, and propane), where L_{vis} is the visible flame length (from the orifice, including any liftoff distance), f_s is the mass fraction of fuel in a stoichiometric mixture of fuel and air (Equation 40), and d_j, ρ_j, and ρ_{amb} are the orifice diameter, density of fuel at the orifice, and density of air, respectively [14]. It is assumed that this curve will also be valid for blends [10]. The curve is given by

$$L^* = \begin{cases} \frac{13.5\text{Fr}_f^{2/5}}{(1+0.07\text{Fr}_f^2)^{1/5}}, & \text{Fr}_f < 5, \\ 23, & \text{Fr}_f > 5, \end{cases} \tag{106}$$

which is a function of the flame Froude number (Fr_f), which is the ratio of buoyancy to momentum forces [14]. The flame Froude number is defined as

$$\text{Fr}_f = \frac{u_j f_s^{3/2}}{\sqrt{g d_j (T_{\text{ad}} - T_{amb})/T_{amb}\sqrt{\rho_j/\rho_{amb}}}}, \tag{107}$$

where g is the gravitational constant, u_j is the velocity of the jet at the orifice, T_{ad} is the adiabatic flame temperature (for a stoichiometric mixture, see Section 3.1.2), and T_{amb} is the ambient temperature. The flame width is constant at $W_f = 0.17 L_{\text{vis}}$ [3, 66, 67].

The total emitted radiative power from a flame, S_{rad}, is related to the total energy in the flame by the radiant fraction [3],

$$S_{\text{rad}} = X_{\text{rad}} \dot{m}_{\text{fuel}} \Delta H_c, \tag{108}$$

where X_{rad} is the radiant fraction, $\dot{m}_{\text{fuel}}$ is the mass flow rate of fuel, and ΔH_c is the heat of combustion (120 MJ/kg for hydrogen, 50 MJ/kg for methane, and 46.4 MJ/kg for propane [50, 51]). The radiant fraction (X_{rad}) varies with the flame residence time (τ_f); the relationship is [68]

$$X_{\text{rad}} = 9.45\times10^{-9}(\tau_f a_p T_{\text{ad}}^4)^{0.47}, \tag{109}$$

where a_p is the Planck-mean absorption coefficient for an optically thin flame. To calculate the absorption coefficient, the absorption coefficients of H_2O and CO_2 are calculated at the adiabatic flame temperature from correlations given by Chmielewski and Gieras [69]. The total Planck-mean absorption coefficient is calculated by averaging the absorption coefficient for all of the products of combustion (only H_2O and CO_2 are radiatively active), weighted by the stoichiometric mole fractions of the products. This results in absorption coefficients similar to those reported by Molina et al. [70] (approximately 0.2 for a hydrogen flame and 0.5 for a methane flame).

The flame residence time can be calculated as

$$\tau_f = \frac{\pi \rho_f W_f^2 L_{\text{vis}} f_s}{12 \dot{m}_{\text{fuel}}}, \tag{110}$$

where ρ_f is the flame density [3]. The flame density is calculated as the density at the adiabatic flame temperature:

$$\rho_f = \frac{p_{amb} W_{\text{mix}}}{R T_{\text{ad}}}, \tag{111}$$

where p_{amb} is the ambient pressure, W_{mix} is the mean molecular weight of the stoichiometric products of combustion in air, and R is the universal gas constant.

The transmissivity, which can reduce the radiated heat flux, is calculated to account for the absorption from water vapor and CO_2 [3], using a correlation from Wayne [71]:

$$\begin{aligned}\tau = 1.006 &- 0.001171\left(\log_{10} X_{H_2O}\right) - 0.02368\left(\log_{10} X_{H_2O}\right)^2 \\ &- 0.03188\left(\log_{10} X_{CO_2}\right) + 0.001164\left(\log_{10} X_{CO_2}\right)^2,\end{aligned} \tag{112}$$

where X_{H_2O} and X_{CO_2} is proportional to the amount of water vapor or CO_2 in the path (dimensionless). These values are calculated by:

$$X_{CO_2} = L \cdot \frac{273}{T} \cdot \frac{c_{CO_2}}{335}, \tag{113}$$

$$X_{H_2O} = R_H \cdot L \cdot S_{\text{mm}} \cdot \frac{2.88651\times10^2}{T}. \tag{114}$$

In these relationships, L is the path length (m) through which the radiative light must travel, T is the ambient temperature (K), c_{CO_2} is the concentration of CO_2 in the atmosphere (ppm, assumed to be 400 ppm), R_H is the fractional relative humidity (ranges from 0–1), and S_{mm} is the saturated water vapor pressure (mm Hg), estimated by the relationship:

$$S_{\text{mm}} = \exp\left(10.386 - \frac{5132}{T}\right). \tag{115}$$

3.4.2. Jet Flame with Buoyancy Correction

A similar model to the jet/plume model described in Section 3.3.1 is also used to describe a flame [3]. The model is described by Ekoto et al. [48]. The major difference between the jet/plume model and the flame model is that rather than the mole fraction, the mixture fraction, shown in Equation 42, is a conserved scalar. Similar assumptions are made for Gaussian profiles of the velocity and mixture fraction:

$$v = v_{cl} \exp\left(-\frac{r^2}{B^2}\right), \tag{116}$$

$$f = f_{cl} \exp\left(-\frac{r^2}{\lambda^2 B^2}\right), \tag{117}$$

with the conservation equations written as

x-centerline:

$$\frac{dx}{dS} = \cos\theta, \tag{118}$$

y-centerline:

$$\frac{dy}{dS} = \sin\theta, \tag{119}$$

continuity:

$$\frac{d}{dS} 2\pi \int_0^\infty \rho v r dr = \rho_{amb} E, \tag{120}$$

x-momentum:

$$\frac{d}{dS} 2\pi \int_0^\infty \rho v^2 \cos\theta r dr = \rho_{amb} E v_{\text{wind}}, \tag{121}$$

y-momentum:

$$\frac{d}{dS} \int_0^\infty \rho v^2 \sin\theta r dr = \int_0^\infty (\rho_{amb} - \rho) g r dr, \tag{122}$$

mixture fraction:

$$\frac{d}{dS} 2\pi \int_0^\infty \rho V f r dr = 0. \tag{123}$$

Note that energy conservation is not included in this formulation, but rather the mixture is assumed to be thermally perfect [3], with combustion calculations shown in Section 3.1.2. These calculations assume that the mixture is always in equilibrium (neglecting heat-losses), which results in a calculation of flame temperature and density as functions of mixture fraction similar to Figure 3-2 (with slight variations depending on the reactant temperature).

Equation 121 does not explicitly set the right-hand side of the x-momentum equation to 0, as is done in the unignited jet/plume model (Equation 79) [11]. While the GUI version of HyRAM+ sets $v_{\text{wind}} = 0$, the Python backend enables specification of a cross-wind velocity, v_{wind}. The Gaussian profiles in Equations 116 and 117 are numerically evaluated out to $5B$ (an estimate of ∞), along with the radial profiles of the density (based off of the mixture fraction), which can be plugged into Equations 118–123 and numerically integrated. This results in a system of six first order differential equations where the independent variable is S and the dependent variables are v_{cl}, B, θ, f_{cl}, x, and y. This system of equations is integrated from the starting point to the distance desired using the LSODA algorithm from the scipy.integrate sub-package [38]. By default, the integration distance is the visible flame length, calculated using the correlations in Equations 105 and 106.

Similar to the nonreacting jet, entrainment in the jet flame is modeled as the sum of momentum and buoyancy contributions (Equation 86) [3]. However, the contributions have modified empirical parameters and calculation methods. The momentum driven entrainment is calculated as

$$E_{mom} = 0.0342 \left(\frac{\pi d_{\text{exp}}^2}{4} \frac{\rho_{\text{exp}} v_{\text{exp}}^2}{\rho_\infty} \right)^{1/2}, \tag{124}$$

and buoyancy driven entrainment is calculated as

$$E_{buoy} = 2\pi\alpha_{buoy} g \sin\theta \frac{\int_0^\infty (\rho_{amb} - \rho) dr}{B v_{cl} \rho_{exit}} \tag{125}$$

where $\alpha_{buoy} = 5.75\times10^{-4}$ [48].

3.4.3. Radiation From a Curved Flame

The radiative heat flux from the buoyancy corrected, curved flame is calculated by a weighted multi-source model [3], similar to that described by Hankinson and Lowesmith [72]. The heat flux at a point along the flame is calculated as

$$q = \tau S_{\text{rad}} \frac{V_F}{A_f}, \tag{126}$$

where S_{rad} is calculated according to Equations 108–110, V_F is the view-factor, proportional to the heat flux transmitted to the observer, τ is the transmissivity, calculated by Equation 112, and A_f is the surface area of the flame. Contributions to the total heat flux are broken up into many (N, generally 50) points along the length of the curved flame, and the weighted average proceeds as

$$\tau \frac{V_F}{A_f} = \sum_{i=1}^{N} \frac{w_i \cos\beta_i}{4\pi D_i^2} \tau_i, \tag{127}$$

where the emitter strength weighting parameter is

$$w_i = \begin{cases} i w_1 & i \le 0.75N \\ \left[n - \frac{n-1}{N-n-1}(i - (n+1)) \right] w_1 & i > 0.75N, \end{cases} \tag{128}$$

with the constraint that $1 \le n \le N$ and $\sum_{i=1}^{N} w_i = 1$. In these equations, D and β are the distance and angle, respectively between the observer and unit normal to the point emitter.

3.4.4. Overpressure in Enclosures

If a confined mixture ignites, significant overpressures can develop within the enclosure or confinement area [3]. Overpressure is calculated assuming that the cause of overpressure is the volume change on combustion pressurizing the enclosure. Within HyRAM+, the models described in Section 3.3.4 are used to calculate the volume of fuel within the layer and entire enclosure. It is assumed that all of the fuel within the flammability limits (in both the jet/plume and the accumulated layer) reacts, and the overpressure is calculated, following Bauwens and Dorofeev [73] as

$$\Delta p = p_0 \left(\left[\left(\frac{V_T + V_{\text{fuel}}}{V_T} \right) \left(\frac{V_T + V_{\text{stoich}}(\sigma - 1)}{V_T} \right) \right]^\gamma - 1 \right), \tag{129}$$

where p_0 is the initial pressure, V_T is the total volume of the enclosure, V_{fuel} is the expanded volume of pure fuel following the release, V_{stoich} is the volume of a stoichiometric mixture of the consumed fuel, σ is the expansion ratio of a stoichiometric fuel-air mixture, and γ is the specific heat ratio of air. The expanded volume is given by $V_{\text{fuel}} = m_{\text{fuel}}/\rho_{\text{fuel}}$ where m_{fuel} is the mass of fuel consumed and ρ_{fuel} is the density of the fuel at ambient conditions. V_{stoich} is V_{fuel} divided by the stoichiometric mole fraction of fuel.

3.4.5. Unconfined Overpressure

If an unconfined mixture ignites after a release has been flowing for some time, an overpressure can be observed as the initial mixture burns [12]. In this context, the overpressure is defined as the pressure above ambient. HyRAM+ has four[13] different methods for calculating the overpressure, each of which requires the calculations from an unconfined and unignited jet/plume as described in Section 3.3.1. Each method calculates an overpressure and possibly impulse as a function of distance, R. The origin for the overpressure/impulse (distance from which R is measured) is the point at which the fuel concentration is assumed to be halfway between the lower and upper flammability limits along the jet streamline. This is assumed to be a reasonable origin location, given the overpressure blast wave will originate from the flammable mixture[14].

BST The Baker-Strehlow-Tang (BST) model is based on blast curves that relate overpressure and impulse to the Mach flame speed [75]. The flammable mass of fuel within the unignited jet/plume (m_{flam}) is first found by volumetrically integrating the product of the mass fraction (Y) and density (ρ) of the jet/plume that is within the flammability limits (Y_{LFL}, Y_{UFL}) along the entire length of the jet/plume streamline coordinate (S) [12], or

$$m_{\text{flam}} = \int_{S=0}^{S=\infty} \left(\int_{r_{Y=Y_{\text{UFL}}}}^{r_{Y=Y_{\text{LFL}}}} \rho Y 2\pi r \, dr \right) dS. \tag{130}$$

The energy within the unignited flammable mixture (E_{flam}) is related to the flammable mass through the relationship

$$E_{\text{flam}} = k_{\text{reflection}} m_{\text{flam}} \Delta H_c \tag{131}$$

where $k_{\text{reflection}}$ is a ground reflection factor (assumed to be 2) and ΔH_c is the heat of combustion of the fuel [75]. The scaled distance is related to the energy through the relationship [75]

$$R^*_{\text{BST}} = \frac{R}{(E_{\text{flam}}/P_{\text{ambient}})^{1/3}}. \tag{132}$$

The scaled overpressure and impulse are related to the scaled distance, based on the Mach flame speed, as shown in Figure 3-4 [75]. The Mach flame speed selection is an important choice for BST model results, and can depend on the fuel being combusted, confinement and congestion of

[13] However, currently only the BST, TNT, and Bauwens models are accessible from the graphical user interface.
[14] This is also roughly consistent with the suggested ignition concentration by Jallais et al. [74] for hydrogen.

the flammable mixture, and other factors [75]. The default value in HyRAM+ for the Mach flame speed is 0.35, based on overpressure observations for unconfined releases of hydrogen [74][15]; this value can be changed by the user.

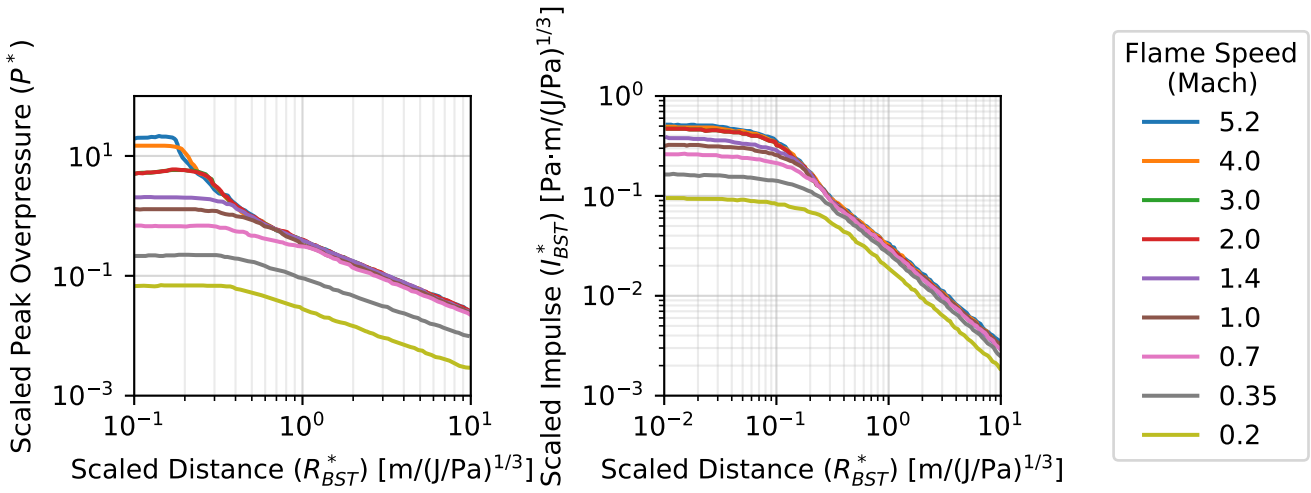

Figure 3-4 Mapping of scaled distance to scaled overpressure (left) and scaled impulse (right) for the BST unconfined overpressure model [11].

The scaled overpressure (P^*) is the peak overpressure (P_s) relative to ambient pressure (P_{ambient}),

$$P^* = P_s / P_{\text{ambient}}, \tag{133}$$

and the impulse (I) is scaled by the flammable energy (E_{flam}), ambient pressure (P_{ambient}), and speed of sound for air ($a_{\text{air}} = 340$ m/s) as

$$I^*_{\text{BST}} = \frac{I a_{\text{air}}}{(E_{\text{flam}} P^2_{\text{ambient}})^{1/3}}. \tag{134}$$

Jallais The Jallais model[16] is based on the work of Jallais et al. [74]. As implemented in HyRAM+, this model is based on the BST model above but with a few modifications. For calculating the flammable mass (see Equation 130), the Jallais model uses flammability limits of 10–75% hydrogen in air rather than the full flammability range for hydrogen of 4-75% [74]. The Jallais model calculates the flame speed (v_f) for use in the BST model based on the mass flow rate ($\dot{m}$) of the leak, as per Equation 135.

$$v_f = \begin{cases} 100 \text{ m/s} & \dot{m} < 0.5 \text{ kg/s} \\ 140 \text{ m/s} & 0.5 \text{ kg/s} < \dot{m} < 1 \text{ kg/s} \\ 240 \text{ m/s} & 1 \text{ kg/s} < \dot{m} < 10 \text{ kg/s} \end{cases} \tag{135}$$

[15]The default Mach flame speed value was 5.2 for HyRAM+ versions 4.0 and 4.1, which is used for detonations; however, experimental observations of unconfined deflagrations seem more applicable for these models.

[16]Currently the Jallais model is not accessible from the graphical user interface, but can be used from the Python package.

The flame speed (v_f) is then used to calculate the Mach flame speed (M_f) for the BST method using the speed of sound in air (a_{air}) in Equation 136.

$$M_f = \frac{v_f}{a_{\text{air}}} \tag{136}$$

The calculated Mach flame speed (M_f) is then used to select the closest (based on absolute value) Mach flame speed curve (see Figure 3-4) for use in the BST method.

As these modifications to the BST method were done specifically for hydrogen, this model is only valid for hydrogen.

TNT The TNT equivalence method is based on finding the mass of TNT that contains the same energy as the fuel being combusted [75]. The flammable mass of fuel within the jet/plume (m_{flam}) is found by volumetrically integrating the product of the mass fraction and density of the jet/plume that is within the flammability limits (see Equation 130) [12]. The flammable mass is scaled by an equivalence factor (F_{equiv}, 3% by default [75]), and the equivalent mass of TNT ($m_{TNT_{equiv}}$) is calculated as

$$m_{\text{TNT}_{\text{equiv}}} = F_{\text{equiv}} \frac{m_{\text{flam}} \Delta H_c}{\Delta H_{c,\text{TNT}}}, \tag{137}$$

where $\Delta H_{c,\text{TNT}} = 4.68$ MJ/kg is the equivalent specific blast energy of TNT[17]. The scaled distance (R^*_{TNT}) is related to the equivalent mass of TNT ($m_{\text{TNT}_{\text{equiv}}}$) through the relationship

$$R^*_{\text{TNT}} = \frac{R}{m^{1/3}_{\text{TNT}_{\text{equiv}}}}, \tag{138}$$

and the scaled overpressure (P^*) and scaled impulse (I^*_{TNT}) resulting from combustion are related to the scaled distance as shown by Figure 3-5.

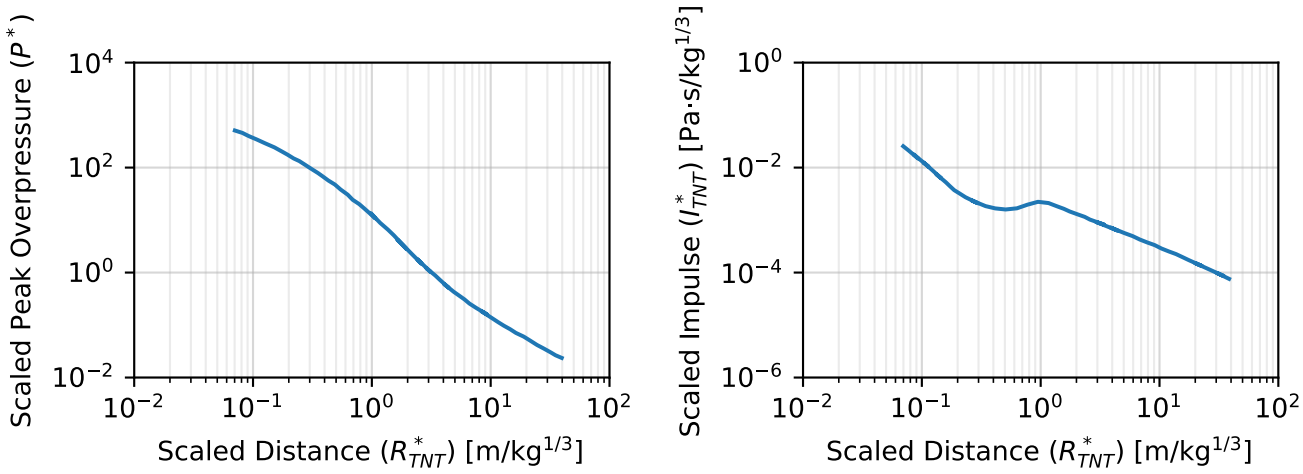

Figure 3-5 Mapping of scaled distance to scaled overpressure (left) and scaled impulse (right) for the TNT equivalence unconfined overpressure model [11].

[17] Previous versions of HyRAM+ (e.g., [11]) had a separate Engineering Toolkit calculation that used a slightly different value for the TNT blast energy.

The scaled overpressure (P^*) is the overpressure (P_s) relative to ambient pressure (see Equation 133), and the impulse (I) is scaled by the third root of the TNT mass ($m_{\mathrm{TNT_{equiv}}}$), or

$$I^*_{\mathrm{TNT}} = \frac{I}{m^{1/3}_{\mathrm{TNT_{equiv}}}}. \tag{139}$$

Bauwens The Bauwens method for unconfined overpressure calculation is based on the work of Bauwens and Dorfeev [76, 77]. In this method, the detonable mass within the unconfined jet/plume is calculated and then the overpressure is based on detonation of that mass of fuel [12]. Due to the dependence of this model on detonation cell size, it has not been updated to work with mixtures/blends yet [10].

The detonation cell size (λ_{det}) is calculated at each point in the jet/plume, based on equivalence ratio (ϕ) and fits to data from the detonation database [78]. The fits to the data are based on a polynomial fit in log-log space [11]:

$$\ln \lambda_{det} = a + b \ln \phi + c(\ln \phi)^2 + d(\ln \phi)^3 + e(\ln \phi)^4, \tag{140}$$

where the parameters a–e are given in Table 3-1. The equivalence ratio (ϕ) is calculated from the mole fraction field (X, see Section 3.3.1) and the stoichiometric fuel to air ratio (FAR_s) as

$$\phi = \frac{X/(1-X)}{\mathrm{FAR}_s} \tag{141}$$

where

$$\mathrm{FAR}_s = \frac{1}{4.76\frac{1+3n_C}{2}}, \tag{142}$$

where n_C is the number of carbon atoms in the fuel.

Table 3-1 Detonation cell size fitted parameters

Fuel	a	b	c	d	e
H_2	2.94771698	-0.16536739	2.2608031	-1.18064551	0.45823461
CH_4	5.768321	1.13938677	113.36802963	0	0
C_3H_8	4.44856885	-0.73108257	5.50526263	0	0

The fits and data for different fuels are shown in Figure 3-6.

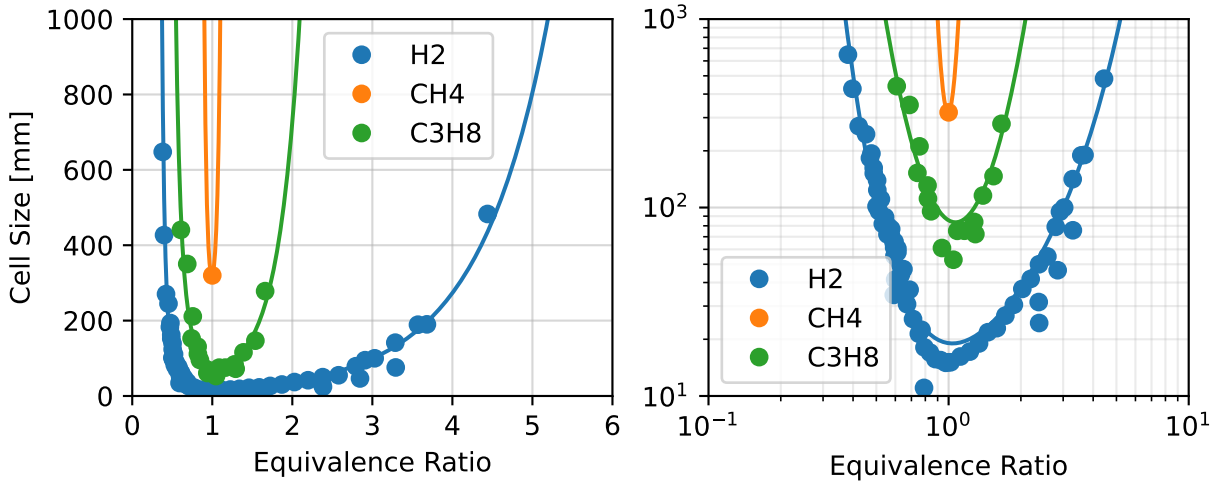

Figure 3-6 Detonation cell size data (points) from the detonation database [78] and fits to the data (lines) on a linear (left) and logarithmic (right) scale [11].

Once the detonation cell size is calculated, the gradient in the radial direction of the detonation cell size ($d\lambda_{det}/dr$) is found numerically [12]. In addition, the number of cells that fit within the layer ($n_{\lambda_{det}}$) is numerically calculated as

$$n_{\lambda_{det}} = \int_0^r \frac{dr}{\lambda_{det}(r)}. \tag{143}$$

Detonations are presumed to propagate in areas that are within the flammability limits, with a detonation cell size gradient less than 0.1 ($d\lambda_{det}/dr < 0.1$), and where there are at least five cells within the layer ($n_{\lambda_{det}} \geq 5$). The mass of fuel within the jet/plume that meets these constraints is calculated as the detonable mass (m_{det}). In equation form,

$$m_{\text{det}} = \int_{S=0}^{\infty} \left(\int_{r=0}^{\infty} \rho Y 2\pi r dr \right) dS, \quad \text{where } Y_{\text{lean}} \leq Y \leq Y_{\text{rich}},\ d\lambda_{det}/dr < 0.1, \text{ and } n_{\lambda_{det}} \geq 5. \tag{144}$$

The dimensionless distance (R^*_{Bauwens}) from the center of the detonable region is calculated as

$$R^*_{\text{Bauwens}} = R \left(\frac{P_{\text{ambient}}}{E_{\text{det}}} \right)^{1/3}, \tag{145}$$

where the energy of detonable fuel (E_{det}) is calculated as

$$E_{\text{det}} = m_{\text{det}} \Delta H_c. \tag{146}$$

Finally, the scaled overpressure (P^*) is calculated as

$$P^* = \frac{0.34}{(R^*_{\text{Bauwens}})^{4/3}} + \frac{0.062}{(R^*_{\text{Bauwens}})^2} + \frac{0.0033}{(R^*_{\text{Bauwens}})^3}. \tag{147}$$

To prevent infinite overpressure calculation and division by zero errors, the scaled distance, R^*, is limited to a minimum value of 0.01 and any scaled distances less than that will use 0.01 in calculation of the scaled overpressure.

There is currently no calculation of impulse for this model. This means that the overpressure probit models in Section 2.4.2 that use impulse cannot be used with this model [12].

4. IMPLEMENTATION DETAILS

4.1. Python Calculation Dependencies

The calculations in HyRAM+ utilize the NumPy and SciPy packages [38, 79, 80]. NumPy provides support for multi-dimensional arrays, mathematical functions of arrays, and some numerical linear algebra routines. SciPy provides a variety of numerical method routines including support for statistical distributions, numerical linear algebra, integration, interpolation, optimization, root-finding, ordinary differential equation solvers, and others. Plots in HyRAM+ are made using Matplotlib [81].

4.2. Unit Conversion

HyRAM+ modules perform calculations using values in the International System of Units (SI) [3]. Conversions are performed in the graphical user interface allowing the user to use units that are preferred or more relevant in problem context, while passing data to the Python calculation algorithms in the expected SI units. Table 4-1 contains the convertible units currently available in HyRAM+, with the SI unit listed first. Note that all pressure units are assumed to be absolute pressure, not gauge pressure.

Table 4-1 HyRAM+ convertible units.

Unit Type	Units Available
Distance	m, mm, in, ft, yd
Area	m^2, cm^2, mm^2, ft^2, in^2, yd^2
Volume	m^3, mm^3, cm^3, mL, L, in^3, ft^3
Angle	rad, deg
Time	s, ms, min, hr
Pressure	Pa, kPa, MPa, psi, atm, bar, J/m^3
Temperature	K, °C, °F,
Speed	m/s
Mass	kg, mg, g, lb
Mass Flow Rate	kg/s
Volumetric Flow Rate	m^3/s

This page intentionally left blank.

REFERENCES

[1] Katrina M. Groth and Andrei V. Tchouvelev. A toolkit for integrated deterministic and probabilistic assessment for hydrogen infrastructure. In *Proceedings of the Probabilistic Safety and Management Conference (PSAM 12)*, Honolulu, HI (USA), June 22-27 2014.

[2] K. M. Groth and E. S. Hecht. HyRAM: a methodology and toolkit for quantitative risk assessment of hydrogen systems. In *Proceedings of the International Conference on Hydrogen Safety (ICHS 2015)*, Yokohama (Japan), October 19-21 2015.

[3] Katrina M. Groth, Ethan S. Hecht, and John T. Reynolds. Methodology for assessing the safety of Hydrogen Systems: HyRAM 1.0 technical reference manual. Technical Report SAND2015-10216, Sandia National Laboratories, November 2015.

[4] Katrina M. Groth and Ethan S. Hecht. HyRAM: A methodology and toolkit for quantitative risk assessment of hydrogen systems. *International Journal of Hydrogen Energy*, 42(11): 7485–7493, 2017.

[5] Michael C. Devin, Brian D. Ehrhart, and Ethan S. Hecht. Validation of HyRAM+ version 5.1 physics models. Technical Report SAND2024-14886, Sandia National Laboratories, October 2024.

[6] Scott Egbert, Xuefang Li, Myra L Blaylock, and Ethan Hecht. Mixing of liquid methane releases. Technical Report SAND2018-13757R, Sandia National Laboratories, 2018.

[7] Myra L. Blaylock, Ethan Hecht, and Cyrus Jordan. Validation of the altram physics models for use with compressed natural gas. Technical Report SAND2019-13408, Sandia National Laboratories, June 2020.

[8] Jessica G. Shum, Ethan S. Hecht, and Myra L. Blaylock. Validation of the HyRAM+ physics models for use with propane. Technical Report SAND2021-3244, Sandia National Laboratories, 2021.

[9] Brian D. Ehrhart, Ethan S. Hecht, Benjamin B. Schroeder, Myra L. Blaylock, Erin E. Carrier, Katrina M. Groth, and John T. Reynolds. Hydrogen Plus Other Alternative Fuels Risk Assessment Models (HyRAM+) Version 5.1 Technical Reference Manual. Technical Report SAND2023-14224, Sandia National Laboratories, December 2023.

[10] Brian D. Ehrhart, Ethan S. Hecht, Myra L. Blaylock, Erin E. Carrier, Katrina M. Groth, and John T. Reynolds. Hydrogen Plus Other Alternative Fuels Risk Assessment Models (HyRAM+) Version 5.0 Technical Reference Manual. Technical Report SAND2022-16425, Sandia National Laboratories, November 2022.

[11] Brian D. Ehrhart, Ethan S. Hecht, Myra L. Blaylock, Erin E. Carrier, Katrina M. Groth, and John T. Reynolds. Hydrogen Plus Other Alternative Fuels Risk Assessment Models (HyRAM+) Version 4.1 Technical Reference Manual. Technical Report SAND2022-5649, Sandia National Laboratories, April 2022.

[12] Ethan S. Hecht, Brian D. Ehrhart, Myra L. Blaylock, Erin E. Carrier, Katrina M. Groth, and John T. Reynolds. Hydrogen Plus Other Alternative Fuels Risk Assessment Models (HyRAM+) Version 4.0 Technical Reference Manual. Technical Report SAND2021-14813, Sandia National Laboratories, November 2021.

[13] Brian D. Ehrhart, Ethan S. Hecht, Myra L. Blaylock, Erin E. Carrier, Katrina M. Groth, and John T. Reynolds. Hydrogen Risk Assessment Models (HyRAM) Version 3.1 Technical Reference Manual. Technical Report SAND2021-5812, Sandia National Laboratories, May 2021.

[14] Brian D. Ehrhart, Ethan S. Hecht, Myra L. Blaylock, Erin E. Carrier, Katrina M. Groth, and John T. Reynolds. Hydrogen Risk Assessment Models (HyRAM) Version 3.0 Technical Reference Manual. Technical Report SAND2020-10600, Sandia National Laboratories, September 2020.

[15] Katrina M. Groth, Ethan S. Hecht, John T. Reynolds, Myra L. Blaylock, and Erin E. Carrier. Methodology for assessing the safety of Hydrogen Systems: HyRAM 1.1 technical reference manual. Technical Report SAND2017-2998, Sandia National Laboratories, March 2017.

[16] Stanley Kaplan and B. John Garrick. On the quantitative definition of risk. *Risk Analysis*, 1 (1):11–27, 1981.

[17] Katrina M. Groth, Jeffrey L. LaChance, and Aaron P. Harris. Early-stage quantitative risk assessment to support development of codes and standard requirements for indoor fueling of hydrogen vehicles. Technical Report SAND2012-10150, Sandia National Laboratories, November 2012.

[18] CGA P-28. OSHA process safety management and epa risk management plan guidance document for bulk liquid hydrogen supply systems. Technical report, Compressed Gas Association, 2014.

[19] Jeffrey LaChance, William Houf, Bobby Middleton, and Larry Fluer. Analyses to support development of risk-informed separation distances for hydrogen codes and standards. Technical Report SAND2009-0874, Sandia National Laboratories, March 2009.

[20] Austin Glover, Austin Baird, and Dusty Brooks. Final report on hydrogen plant hazards and risk analysis supporting hydrogen plant siting near nuclear power plants. Technical Report SAND2020-7946, Sandia National Laboratories, July 2020.

[21] Dusty M. Brooks, Brian D. Ehrhart, and Chris LaFleur. Development of liquid hydrogen leak frequencies using a Bayesian update process. In *2021 International Conference on Hydrogen Safety*, September 2021.

[22] Dusty Brooks, Austin Glover, and Brian D. Ehrhart. Compressed natural gas component leak frequency estimation. Technical Report SAND2022-14164, Sandia National Laboratories, October 2022.

[23] Garrett W. Mulcahy, Dusty M. Brooks, and Brian D. Ehrhart. Using Bayesian methodology to estimate liquefied natural gas leak frequencies. Technical Report SAND2021-4905, Sandia National Laboratories, April 2021.

[24] Dusty Brooks and Brian D. Ehrhart. LPG component leak frequency estimation. Technical Report SAND2023-05818, Sandia National Laboratories, August 2023.

[25] Dusty Brooks, Melissa S. Louie, and Brian D. Ehrhart. Updated filter leak frequencies for use in risk assessments. Technical Report SAND2024-06491, Sandia National Laboratories, May 2024.

[26] Andrei V. Tchouvelev. Knowledge gaps in hydrogen safety: A white paper. Technical report, International Energy Agency Hydrogen Implementing Agreement Task 19, January 2008.

[27] TNO. Methods for the determination of possible damage. Technical Report CPR 16E, The Netherlands Organization of Applied Scientific Research (TNO), 1992.

[28] Phani K. Raj. A review of the criteria for people exposure to radiant heat flux from fires. *Journal of Hazardous Materials*, 159(1):61–71, 2008.

[29] N. A. Eisenberg, C. J. Lynch, and R. J. Breeding. Vulnerability model. A simulation system for assessing damage resulting from marine spills. Technical Report SA/A-015 245, U.S. Coast Guard, 1975.

[30] C. K. Tsao and W. W. Perry. Modifications to the vulnerability model: a simulation system for assessing damage resulting from marine spills. Technical Report ADA 075 231, U.S. Coast Guard, 1979.

[31] F. P. Lees. The assessment of major hazards: a model for fatal injury from burns. *Process Safety and Environmental Protection*, 72(3):127–134, 1994.

[32] Jeffrey LaChance, Andrei Tchouvelev, and Angunn Engebø. Development of uniform harm criteria for use in quantitative risk analysis of the hydrogen infrastructure. *International Journal of Hydrogen Energy*, 36(3):2381–2388, February 2011.

[33] Center for Chemical Process Safety (CCPS). *Guidelines for Chemical Process Quantitative Risk Analysis*. American Institute of Chemical Engineers, 1999.

[34] HSE. *Major hazard aspects of the transport of dangerous substances*. UK Health and Safety Executive, 1991.

[35] UK Health and Safety Executive. Methods of approximation and determination of human vulnerability for offshore major accident hazard assessment. Technical report, UK Health and Safety Executive, 2010.

[36] Benjamin B. Schroeder and Dusty M. Brooks. Uncertainty quantification and sensitivity analysis for quantitative risk assessments of hydrogen infrastructure. Technical Report SAND2024-09878, Sandia National Laboratories, 2024.

[37] Michael D. McKay. Latin hypercube sampling as a tool in uncertainty analysis of computer models. In *Proceedings of the 1992 Winter Simulation Conference*, pages 557–564, 1992.

[38] Pauli Virtanen, Ralf Gommers, Travis E. Oliphant, Matt Haberland, Tyler Reddy, David Cournapeau, Evgeni Burovski, Pearu Peterson, Warren Weckesser, Jonathan Bright, Stéfan J. van der Walt, Matthew Brett, Joshua Wilson, K. Jarrod Millman, Nikolay Mayorov, Andrew R. J. Nelson, Eric Jones, Robert Kern, Eric Larson, CJ Carey, İlhan Polat, Yu Feng, Eric W. Moore, Jake VanderPlas, Denis Laxalde, Josef Perktold, Robert Cimrman, Ian Henriksen, E. A. Quintero, Charles R Harris, Anne M. Archibald, Antônio H. Ribeiro, Fabian Pedregosa, Paul van Mulbregt, and SciPy 1.0 Contributors. SciPy 1.0: Fundamental Algorithms for Scientific Computing in Python. *Nature Methods*, 17:261–272, 2020.

[39] Ian H. Bell, Jorrit Wronski, Sylvain Quoilin, and Vincent Lemort. Pure and Pseudo-pure Fluid Thermophysical Property Evaluation and the Open-Source Thermophysical Property Library CoolProp. *Industrial & Engineering Chemistry Research*, 53(6):2498–2508, February 2014. doi: 10.1021/ie4033999.

[40] J. W. Leachman, R. T. Jacobsen, S. G. Penoncello, and E. W. Lemmon. Fundamental equations of state for parahydrogen, normal hydrogen, and orthohydrogen. *Journal of Physical and Chemical Reference Data*, 38(3):721–748, September 2009.

[41] U. Setzmann and W. Wagner. A new equation of state and tables of thermodynamic properties for methane covering the range from the melting line to 625 K at pressures up to 100 MPa. *Journal of Physical and Chemical Reference Data*, 20(6):1061–1155, 1991.

[42] Eric W. Lemmon, Mark O. McLinden, and Wolfgang Wagner. Thermodynamic properties of propane. III. A reference equation of state for temperatures from the melting line to 650 K and pressures up to 1000 MPa. *Journal of Chemical & Engineering Data*, 54(12): 3141–3180, 2009.

[43] O. Kunz, R. Klimeck, W. Wagner, and M. Jaeschke. *The GERG-2004 wide-range equation of state for natural gases and other mixtures*. VDI Verlag GmbH, Jul 2007. ISBN 978-3-18-355706-6.

[44] O. Kunz and W. Wagner. The GERG-2008 wide-range equation of state for natural gases and other mixtures: An expansion of GERG-2004. *Journal of Chemical & Engineering Data*, 57 (11):3032–3091, 2012. doi: 10.1021/je300655b.

[45] Eric W. Lemmon and Richard T. Jacobsen. A generalized model for the thermodynamic properties of mixtures. *International Journal of Thermophysics*, 20:825–835, 1999. doi: 10.1023/A:1022627001338.

[46] Eric W. Lemmon, Richard T. Jacobsen, Steven G. Penoncello, and Daniel G. Friend. Thermodynamic properties of air and mixtures of nitrogen, argon, and oxygen from 60 to 2000 K at pressures to 2000 MPa. *Journal of Physical and Chemical Reference Data*, 29(3): 331–385, 2000. doi: 10.1063/1.1285884.

[47] Eric W. Lemmon and Richard T. Jacobsen. Equations of state for mixtures of r-32, r-125, r-134a, r-143a, and r-152a. *Journal of Physical and Chemical Reference Data*, 33(2): 593–620, 2004. doi: 10.1063/1.1649997.

[48] I. W. Ekoto, A. J. Ruggles, L. W. Creitz, and J. X. Li. Updated jet flame radiation modeling with buoyancy corrections. *International Journal of Hydrogen Energy*, 39(35): 20570–20577, December 2014.

[49] National Institute of Standards and Technology. NIST Chemistry WebBook, SRD 69. `https://webbook.nist.gov/chemistry/`.

[50] Sam Mannan, editor. *Lees' Loss Prevention in the Process Industries*. Elsevier Science & Technology, 3rd edition, 2005.

[51] Morgan J. Hurley, Daniel T. Gottuk, John R. Hall Jr., Kazunori Harada, Erica D. Kuligowski, Milosh Puchovsky, Jose´ L. Torero, John M. Watts Jr., and Christopher J. Wieczorek, editors. *SFPE Handbook of Fire Protection Engineering*. Springer, New York, NY, 5th edition, 2016.

[52] J.R. Travis, D. Piccioni Koch, and W. Breitung. A homogeneous non-equilibrium two-phase critical flow model. *International Journal of Hydrogen Energy*, 37(22):17373–17379, 2012.

[53] Tom Spicer and Derek Miller. Quantifying the mass discharge rate of flashing two phase releases through simple holes to the atmosphere. *Process Safety Progress*, 37(3):382–396, 2018.

[54] Alexandros G. Venetsanos. Homogeneous non-equilibrium two-phase choked flow modeling. *International Journal of Hydrogen Energy*, 43(50):22715–22726, 2018.

[55] K. Bülent Yüceil and M. Volkan Ötügen. Scaling parameters for underexpanded supersonic jets. *Physics of Fluids*, 14(12):4206–4215, October 2002.

[56] A. D. Birch, D. J. Hughes, and F. Swaffield. Velocity decay of high pressure jets. *Combustion Science and Technology*, 52(1-3):161–171, 1987.

[57] A. D. Birch, D. R. Brown, M. G. Dodson, and F. Swaffield. The structure and concentration decay of high pressure jets of natural gas. *Combustion Science and Technology*, 36(5-6): 249–261, 1984.

[58] B. C. R. Ewan and K. Moodie. Structure and velocity measurements in underexpanded jets. *Combustion Science and Technology*, 45(5-6):275–288, 1986.

[59] V. Molkov, D. Makarov, and M. Bragin. Physics and modelling of under-expanded jets and hydrogen dispersion in atmosphere. In *Proceedings of the 24th International Conference on Interaction of Intense Energy Fluxes with Matter*, March 1-6 2009.

[60] W.G. Houf and W.S. Winters. Simulation of high-pressure liquid hydrogen releases. *International Journal of Hydrogen Energy*, 38(19):8092–8099, June 2013. doi: 10.1016/j.ijhydene.2013.01.052.

[61] W. Houf and R. Schefer. Analytical and experimental investigation of small-scale unintended releases of hydrogen. *International Journal of Hydrogen Energy*, 33(4): 1435–1444, February 2008.

[62] W. S. Winters. Modeling leaks from liquid hydrogen storage systems. Technical Report SAND2009-0035, Sandia National Laboratories, January 2009.

[63] M. Hosseini, I. Dincer, G.F. Naterer, and M.A. Rosen. Thermodynamic analysis of filling compressed gaseous hydrogen storage tanks. *International Journal of Hydrogen Energy*, 37 (6):5063–5071, March 2012. doi: https://doi.org/10.1016/j.ijhydene.2011.12.047.

[64] B.J. Lowesmith, G. Hankinson, C. Spataru, and M. Stobbart. Gas build-up in a domestic property following releases of methane/hydrogen mixtures. *International Journal of Hydrogen Energy*, 34(14):5932–5939, July 2009.

[65] William Houf and Robert Schefer. Predicting radiative heat fluxes and flammability envelopes from unintended releases of hydrogen. *International Journal of Hydrogen Energy*, 32(1):136–151, January 2007.

[66] Stephen R. Turns and Franklin H. Myhr. Oxides of nitrogen emissions from turbulent jet flames: Part I—fuel effects and flame radiation. *Combustion and Flame*, 87(3):319–335, 1991.

[67] R. W. Schefer, W. G. Houf, B. Bourne, and J. Colton. Spatial and radiative properties of an open-flame hydrogen plume. *International Journal of Hydrogen Energy*, 31(10):1332–1340, 2006.

[68] Pratikash P. Panda and Ethan S. Hecht. Ignition and flame characteristics of cryogenic hydrogen releases. *International Journal of Hydrogen Energy*, 42(1):775–785, January 2017.

[69] Maciej Chmielewski and Marian Gieras. Planck mean absorption coefficients of H_2O, CO_2, CO and NO for radiation numerical modeling in combusting flows. *Journal of Power Technologies*, 95(2):97–104, 2015.

[70] Alejandro Molina, Robert W. Schefer, and William G. Houf. Radiative fraction and optical thickness in large-scale hydrogen-jet fires. *Proceedings of the Combustion Institute*, 31(2): 2565–2572, January 2007.

[71] F. David Wayne. An economical formula for calculating atmospheric infrared transmissivities. *Journal of Loss Prevention in the Process Industries*, 4(2):86 – 92, January 1991. ISSN 0950-4230. doi: http://dx.doi.org/10.1016/0950-4230(91)80012-J.

[72] Geoffrey Hankinson and Barbara Joan Lowesmith. A consideration of methods of determining the radiative characteristics of jet fires. *Combustion and Flame*, 159(3): 1165–1177, March 2012.

[73] C.R. Bauwens and S.B. Dorofeev. CFD modeling and consequence analysis of an accidental hydrogen release in a large scale facility. *International Journal of Hydrogen Energy*, 39(35): 20447–20454, December 2014.

[74] Simon Jallais, Elena Vyazmina, Derek Miller, and J. Kelly Thomas. Hydrogen jet vapor cloud explosion: A model for predicting blast size and application to risk assessment. *Process Safety Progress*, 37(3):397–410, 2018.

[75] Center for Chemical Process Safety. *Guidelines for Vapor Cloud Explosion, Pressure Vessel Burst, BLEVE, and Flash Fire Hazards*. John Wiley & Sons Ltd., 2010.

[76] C. Regis L. Bauwens and Sergey B. Dorofeev. Modeling detonation limits for arbitrary non-uniform concentration distributions in fuel–air mixtures. *Combustion and Flame*, 221: 338–345, 2020.

[77] C. Regis L. Bauwens and Sergey B. Dorofeev. Quantifying the potential consequences of a detonation in a hydrogen jet release. In *Proceedings of the International Conference on Hydrogen Safety (ICHS 2019)*, pages 612–623, Adelaide (Austrailia), September 24 - 26 2019.

[78] California Institute of Technology and Joseph E. Shepherd. Detonation Database. `https://shepherd.caltech.edu/detn_db/html/db_10.html`.

[79] Travis E. Oliphant. *A guide to NumPy*, volume 1. Trelgol Publishing USA, 2006.

[80] Stefan Van Der Walt, S. Chris Colbert, and Gael Varoquaux. The NumPy array: a structure for efficient numerical computation. *Computing in Science & Engineering*, 13(2):22, 2011.

[81] J. D. Hunter. Matplotlib: A 2D graphics environment. *Computing in Science & Engineering*, 9(3):90–95, 2007. doi: 10.1109/MCSE.2007.55.

This page intentionally left blank.

DISTRIBUTION

Email—Internal

Name	Org.	Sandia Email Address
Ethan Hecht	8367	ehecht@sandia.gov
Kristin Hertz	8367	klhertz@sandia.gov
Brian Ehrhart	8854	bdehrha@sandia.gov
Chris LaFleur	8854	aclafle@sandia.gov
Michael Devin	8921	mcdevin@sandia.gov
Technical Library	1911	sanddocs@sandia.gov

Email—External

Name	Company Email Address	Company Name
Alex Gupta	algupta@epri.com	EPRI
Laura Hill	laura.hill@ee.doe.gov	DOE EERE HFTO
David Park	dpark@h2fcp.org	H2FCP
Annette Rohr	ARohr@epri.com	EPRI
Christine Watson	christine.watson@ee.doe.gov	DOE EERE HFTO

This page intentionally left blank.

This page intentionally left blank.

Sandia National Laboratories is a multimission laboratory managed and operated by National Technology & Engineering Solutions of Sandia LLC, a wholly owned subsidiary of Honeywell International Inc., for the U.S. Department of Energy's National Nuclear Security Administration under contract DE-NA0003525.